Early Stopping in Experimentation with Real-time Functional Magnetic Resonance Imaging Using a Modified Sequential Probability Ratio Test

Sarah J. A. Carr[1,2], Weicong Chen[3], Jeremy Fondran[4], Harry Friel[5], Javier Sanchez-Gonzalez[6], Jing Zhang[4] and Curtis Tatsuoka[4,2,*]

1. Department of Neuroimaging, Institute of Psychiatry, Psychology and Neuroscience, King's College London, UK
2. Department of Neurology, Case Western Reserve University, Cleveland, OH, USA
3. Department of Computer and Data Sciences, Case Western Reserve University, Cleveland, OH, USA
4. Department of Population and Quantitative Health Sciences, Case Western Reserve University, Cleveland, OH, USA
5. Philips Healthcare, Highland Heights, OH, USA
6. Philips Healthcare, Madrid, Spain

*Corresponding Author:
Curtis Tatsuoka
10900 Euclid Avenue
Case Western Reserve University
Cleveland, OH, USA 44106
Email: cmt66@case.edu

KEY WORDS: real-time fMRI, adaptive fMRI, dynamic experimentation, SPRT, early stopping

Abstract

Introduction: Functional magnetic resonance imaging (fMRI) often involves long scanning durations to ensure the associated brain activity can be detected. However, excessive experimentation can lead to many undesirable effects, such as from learning and/or fatigue effects, discomfort for the subject, excessive motion artifacts and loss of sustained attention on task. Overly long experimentation can thus have a detrimental effect on signal quality and accurate voxel activation detection. Here, we propose dynamic experimentation with real-time fMRI using a novel statistically-driven approach that invokes early stopping when sufficient statistical evidence for assessing the task-related activation is observed.

Methods: Voxel-level sequential probability ratio test (SPRT) statistics based on general linear models (GLMs) were implemented on fMRI scans of a mathematical 1-back task from 12 healthy teenage subjects and 11 teenage subjects born extremely preterm (EPT). This approach is based on likelihood ratios and allows for systematic early stopping based on statistical error thresholds. We adopt a two-stage estimation approach that allows for accurate estimates of GLM parameters before stopping is considered. Early stopping performance is reported for different first stage lengths, and activation results are compared with full durations. Finally,

group comparisons are conducted with both early stopped and full duration scan data. Numerical parallelization was employed to facilitate completion of computations involving a new scan within every repetition time (TR).

Results: Use of SPRT demonstrates the feasibility and efficiency gains of automated early stopping, with comparable activation detection as with full protocols. Dynamic stopping of stimulus administration was achieved in around half of subjects, with typical time savings of up to 33% (4 minutes on a 12 minute scan). A group analysis produced similar patterns of activity for control subjects between early stopping and full duration scans. The EPT group, individually, demonstrated more variability in location and extent of the activations compared to the normal term control group. This was apparent in the EPT group results, reflected by fewer and smaller clusters.

Conclusion: A systematic statistical approach for early stopping with real-time fMRI experimentation has been implemented. This dynamic approach has promise for reducing subject burden and fatigue effects.

1.0 Introduction

Analysis of task-based fMRI scans is typically performed with fixed, predetermined experimental designs. As a result, subjects must often endure stimulus protocols that are overly long in order to ensure the neural activity can be statistically discerned in the noisy data. However, this can lead to fatigue, learning effects and excessive motion, such as from agitation, as well as being costlier to administer due to longer scan times and potentially less reliable measurement. Also, the experimenter does not know if the neural activity is detectable until long after the scanning session is over. Real-time functional MRI (RT-fMRI) provides an opportunity to ameliorate these issues. RT-fMRI has been successfully applied in the field of neurofeedback and biofeedback from neural responses, where subjects may be trained to alter their brain activity based on real-time information provided from the fMRI scans. This has been reported in ADHD (1), healthy subjects with no psychiatric or neurological disorders (2, 3), Alzheimer's disease (4) and Parkinson's disease (5, 6). Its uses have also been described in psychoradiology to aid diagnosis and treatment planning in psychiatric disorders (7). Real-time resting state fMRI has for instance been studied and implemented as well using TurboFIRE (8). A largely unexplored application of RT-fMRI is to dynamically and statistically determine when a stimulus has been sufficiently presented in terms of replication of blocks to terminate early. The magnitude of effort and variability in neural activity while completing a task will vary from person to person. Trial administration within a block design can be stopped early if sequentially updated statistical inference on activation can be determined with sufficient accuracy based on the observed BOLD (blood oxygen level dependent) signal response up to that point. This application will be explored in detail.

The benefits of adaptive RT-fMRI include: 1) <u>Shorter scan times for fMRI testing</u>: Shorter scan times cannot only save in technology and personnel costs, but fatigue and learning effects can be avoided, improving signal quality. Scanning becomes less burdensome on the subject as

well, which is an especially important consideration for children or elderly subjects. 2) Real-time quality control: greater consistency in activation classification error can be obtained, through statistical error-based benchmarks for stopping rules and real-time feedback on classification performance and adjustment of stimulus durations. 3) Richer information: Paradigms can become more complex and sophisticated. With greater time efficiency and flexibility, more variations of a stimulus, such as reflected by a broader range of difficulty levels, can be administered in the same amount of time. 4) Wide applicability: Dynamic adjustment of stimuli based on BOLD response in real time can be generally applied across a range of focus areas that investigate localization of brain activity, including cognition and motor functioning.

Since the advent of RT-fMRI in the mid 1990's (9), a handful of mainstream software packages have been developed for use by the fMRI community. These include Turbo BrainVoyager (10), AFNI's real-time plugin (9) and FSL-based FRIEND (11). There have been a few previous studies that have employed adaptive task-based RT-fMRI. In one example, it has been used to determine 'good' and 'bad' brain states to optimize learning (12). The presentation of novel scenes was prompted by the detection of 'good' brain states; the 'good' template was determined based on a prior standard acquisition test scan. They used real-time general linear model (GLM) methods described in (13) to estimate the BOLD signal magnitude at each time point (each scan) and compared it to a value within a region of interest from the earlier test scan. Another adaptive RT-fMRI study has used a person's brain state to judge their attention to a task (14). When their attention appeared to wander, the difficulty of the task was increased bringing their attention back. The authors applied multivariate pattern analysis to determine task-relevant and task-irrelevant activity. In another example, Lorenz et al (2016) ran FSL to pre-process the scans in real-time before applying a GLM-based analysis. Their study involved eliciting activity in particular brain regions by presenting stimuli chosen based on the response to the previous stimulus. The aim was not to investigate brain activity related to a particular task but simply activate a brain region (15). Another example of adaptive RT-fMRI implemented a Bayesian optimization algorithm to estimate when brain activity was mapped to a particular network (16). The Bayesian optimization was trained on 4 difficulty levels of a task prior to switching to choosing the optimal difficulty levels to elicit the desired activity, where there were 12 other levels to choose from.

Here, we extend the use of a statistically-based dynamic approach to RT-fMRI experimentation described in (17), addressing issues related to practical implementation. This approach involves the sequential updating of voxel-level likelihood ratio tests, known as sequential probability ratio tests (SPRTs) and assessing after each scan whether there is sufficient statistical evidence to determine whether or not an associated parameter value indicates task activation. Such results, considered in aggregate across a collection of voxels, can be used as a basis for early stopping of experimentation. Most off-line, post-hoc analyses of fMRI data use the general linear model to test statistical associations of voxel activation magnitude to task administration (18-20). This approach involves the voxel-level estimation of task-related regression parameters that indicate magnitude of association between an expected hemodynamic response signal from a task and the observed BOLD signal. We have adapted this general method for real-time fMRI by sequentially updating GLM regression parameter estimates as soon as the brain

volumes are collected. At the individual voxel level, we can then assess hypothesis tests related to activation that are based on these estimates. In aggregate, the voxel level analyses inform decisions on early stopping and the tailoring of fMRI experimentation (17).

In comparison to (17), we adopt a two-stage estimation approach that allows for the alternative hypothesis test parameter values that represent activation thresholds to be formulated in terms of z-score scale at the voxel level. This adaptive specification avoids the intractable problem of pre-specifying magnitudes of GLM parameter values that would be considered as "active". Such magnitudes need to be scaled relative to error variance, which is estimated in a first stage. We determine an appropriate duration of the first stage by monitoring estimation convergence of key GLM parameters. Also, while in (17) serial independence was assumed, here we use the "sandwich" estimator to recognize serial covariance in inference (21, 22). The impact of early stopping on group analysis is considered here as well. Importantly, we now present a novel workflow to apply and implement these methods on a Philips scanner, with a dynamic feedback system that allows for real-time dynamic adjustment of the experimentation with subjects. This was facilitated with adoption of numerical parallelization techniques. This work supports the premise that adaptive, individualized experimentation is feasible and can lead to practical and useful savings in scan times by reducing experimental redundancy.

Another novel aspect of this work is the application of adaptive RT-fMRI in a sample group of 12 healthy adolescent subjects and 11 adolescents born extremely preterm (EPT). The fMRI stimulus was a mathematical version of the well-known 1-back task. Early stopping was implemented using sequential probability ratio test (SPRT) statistics and our server was a Linux workstation located in a nearby building. Processing of RT-fMRI was completed within 3 seconds before the next scan arrived. We observed time savings of up to 33 % based on early stopping when 80% of voxels were classified, which equals up to 4 minute savings with a 12-minute scan. The impact on activation analysis from the selection of early stopping criteria is assessed, as described in detail below. Finally, we conduct a comparison of group analyses between EPT versus healthy controls, to assess the effects of early stopping in this context.

2.0 Background Information

2.1 General linear model

Briefly, the general linear model involves convoluting a double gamma hemodynamic response function (HRF) with task indicator variables that denote timing of administration to reflect expected task-related BOLD responses. Voxel-level task-related regression parameters are estimated and represent the association of the observed response to expected task-activated BOLD signal. Thus, activation is assessed through statistical inference on regression parameters. For a given voxel up to time t (i.e. for scans 1 through t), the GLM takes the form:

$$Y_t = X_t B + E_t \tag{1.1}$$

Where Y_t is a $t \times 1$ vector of observed BOLD signal intensities for the voxel up to time t, and E_t is a $t \times 1$ vector that represents the error components. X_t is a $t \times p$ design matrix and includes the expected BOLD signal values per task. We also include cosine functions of increasing periodicity

(scan duration*2, scan duration, scan duration/1.5, scan duration/2 and scan duration/2.5) to model physiological and other low frequency noise (23). For large periodicities, cosine functions are approximately linear for the time frame of scans we consider here, and hence are essentially collinear from a GLM modeling perspective. Five regressors were thus added to the design matrix. $B = \left[b_1 \dots b_j \dots b_p\right]^t$, a p × 1 regression coefficients vector. In this formulation, a regression parameter b_j can represent magnitude of association with task j. E_t is assumed to be distributed as multivariate normal with mean zero and covariance W_t, where W_t is a $t \times t$ matrix that represents the temporal autocorrelation structure. For spatial correlation, we conduct spatial smoothing, so do not explicitly model the spatial correlation structure. Y_t is assumed to have a multivariate normal probability distribution as follows:

$$f(Y_t, B, \sigma^2 W_t) = \frac{1}{(2\pi)^{t/2}|\sigma^2 W_t|}\exp\left(-\frac{1}{2}(Y_y - X_t B)'(\sigma^2 W_t)^{-1}(Y_t - X_t B)\right) \qquad (1.2)$$

where $|\sigma^2 W_t|$ is the determinant of $\sigma^2 W_t$. Major sources of noise in fMRI data include brain metabolism, physiology, and spontaneous fluctuations (24).

We fit regression models in parallel for all voxels under consideration in a target region of interest (ROI), which could include the whole brain. Real-time analysis requires signal and image processing steps, as well as the continual updating of statistical estimates as new scan data are received from the scanner. Hence, given the large number of voxels to be analyzed, real-time fMRI presents “big data” computational challenges.

2.2 Sandwich Estimator

In our previous work (17), we assumed serial independence for computational simplicity. Here we recognize potential serial correlation using the nonparametric sandwich estimator $\widehat{var}\left[c\hat{\beta}\right]$ for contrast c (21, 22). The sandwich estimator is a robust, model-free variance estimator that does not require distributional assumptions. Importantly, it still provides asymptotically consistent variance estimates, although convergence rates can be slow (21, 22). The approach is computational feasible for real time analysis.

2.3 Wald’s Sequential Probability Ratio Test

At the voxel level, we can use the sequential analytic framework of (17, 25-29), to adaptively assess activation status using real-time fMRI. As we will demonstrate, Wald’s SPRT test statistic can serve as the basis of an efficient, sequential testing approach that can greatly reduce the need for experimental block administrations compared with fixed designs while attaining similar classification performance in simulation, and activation patterns with subject data. This approach relies on a SPRT statistic to conduct hypothesis testing, with the null hypothesis representing no activation with respect to a task, and the alternative hypothesis representing some threshold of activation, as represented by a GLM parameter value (17). This statistic is updated with each new observation, and its value is compared with thresholds for stopping.

The general procedure of Wald's SPRT is described as follows. Consider a one-sided hypothesis of the form $H_0: c'\beta = c'\beta_0$ versus $H_a: c'\beta \geq c'\beta_1$, where $c'(\beta_1 - \beta_0) \geq 0$. Two-sided formulations are described in (25) and (17). Implementation of Wald's SPRT involves updating Wald's likelihood ratio statistic as new data are observed (25):

$$\Lambda_t = log\left(\frac{f\left(Y_t|c'\beta_1, \widehat{var}\left[c\hat{\beta}\right]\right)}{f\left(Y_t|c'\beta_0, \widehat{var}\left[c\hat{\beta}\right]\right)}\right) \tag{1.3}$$

where $f(Y|c'\beta_0, \widehat{var}\left[c\hat{\beta}\right])$ and $f(Y|c'\beta_1, \widehat{var}\left[c\hat{\beta}\right])$ are the respective probability densities functions of Y_t given $c'\beta_0$ or $c'\beta_1$ is the true value of parameter of interest and conditioning on the estimated covariance. After Y_t is observed at a time point, t, one of three possible decisions is made according to the following rules:

1. Continue sampling if $B < \Lambda_t < A$
2. Stop sampling and accept H_0 if $\Lambda_t < B$
3. Stop sampling and accept H_a if $A < \Lambda_t$

where stopping boundaries (A, B) = ($\log((1-\beta_E)/\alpha_E)$, $\log(\beta_E/(1-\alpha_E))$), and the target Type I and Type II error levels are respectively denoted as α_E and β_E. These error levels are specified before testing. Note that both the Type I and Type II error levels are controlled for with SPRT, as opposed to standard hypothesis test formulations that only control for Type I error level. Multiple SPRTs are conducted concurrently across voxels and boundary error levels can be adjusted for instance by Bonferroni correction to account for this simultaneous testing.

A practical modification of the original SPRT formulation for stopping is to consider the truncated SPRT (30), which will additionally call for stopping if an upper bound for the number of observations is reached. In our case, this is reached when a fixed number of blocks have been administered. Additional modifications include conducting two-stage estimation to allow sufficient observation for preliminary estimates of the voxel-level error variance from a first stage where stopping is not yet considered (31). With these estimates, we can derive an alternative hypothesis value for a linear contrast of task parameters $c'\beta$ that will correspond to a desired z-statistic value. As an illustration, suppose a z-statistic value of 3.10 is selected, as will be done below in our studies. Note 3.10 is the one-sided p-value = 0.001 - critical value for the standard normal distribution. Given an estimated value $\widehat{\sigma_t}^2$ from a first stage of length t scans, we solve for the value of $\theta_t = c'\beta$ that satisfies $\frac{\theta_t}{\sqrt{\widehat{var}[c'\beta]}} = 3.10$, where X_t is the design matrix up to scan t. This value becomes the alternative hypothesis, and it represents the voxel-level targeted activation magnitude threshold. We update the value of θ_t and $\widehat{\sigma^2}$at each scan, so that the alternative hypothesis is actually dynamic, since the estimation variance for $c'\hat{\beta}$ changes as well.

Ultimately, we aggregate the findings of the voxel-level SPRTs to determine whether or not experimentation within a block design should be terminated early. A "global" stopping rule that considers all voxels in a region of interest (can be whole brain or smaller ROIs) that we have adopted is to terminate task administration when a predetermined percentage of voxels have been classified by their respective SPRTs. For instance, we have used 80% as a global stopping criterion. Note that 80% classified means either as active or non-active. We choose this cut-off as it is fairly strict, and yet approximately one half of the participants still stop early. As we will see, it also facilitates correspondence with full scan data results, particularly if the activation threshold is adjusted to recognize longer scan durations. We also consider other global stopping criterion here, 70% and 90%, and assess impact on stopping times and resultant images arising from early stopping. We also choose Type I and Type II error levels that are relatively more stringent for Type I error. Note that for $c'\beta$ parameter values that are "in-between" the null and alternative hypothesis values, the SPRT is indifferent to preferring one hypothesis over the other. This leads to larger numbers of scans needed before a stopping boundary is crossed. So, we have to accept a lack of decisive stopping decisions for these cases in order for overall experimentation to stop early, even as θ_t decreases as t increases. This can be an acceptable trade-off for shorter experimental scan times and the ability to tailor experimentation.

In sum, we propose that the important design parameters for implementation are selected through analysis of a training sample. For training, each subject undergoes the full duration of experimentation. We consider selection through the following criteria: 1) First stage duration: It is desirable for the voxel-level error variance and beta parameter estimates to stabilize – we assess this qualitatively by assessing plots from a sample of voxels. 2) A z-score activation threshold based at the end of the first stage: we choose a z-score threshold of 3.10 after the first stage since this is a standard threshold value for determining activation of a voxel. Note that thresholds at earlier scans correspond to even larger z-score thresholds at later durations, as we discuss below. 3) Type I and Type II error levels: We want to observe some level of early stopping based on these parameters while the corresponding activation maps with early stopping appear have correspondence to full duration scans (after threshold adjustment for larger number of scans). 4) Global stop rule percentage: a percentage level is selected by relying on similar guidance as when selecting the hypothesis testing error levels.

3.0 Methodology

3.1 Participants

Twelve healthy subjects were recruited, 7 males. They were aged 15-16 years old and 11 were right-handed. They had no known neurological conditions and a normal developmental history. A group of 11 adolescents born EPT were also recruited, 1 male. EPT is defined as being born at < 26-week gestation and weighing < 1000g. All were aged 15-17 years old and 8 were right-handed, 2 left-handed and 1 ambidextrous. All subjects were recruited as part of a larger study to evaluate functional and structural differences associated with mathematical abilities and working memory between those born EPT and those born at normal term. The aim of the larger study is to improve our understanding of mathematics disabilities and potentially lead to

299 improvements in pedagogical practices for young people experiencing problems acquiring
300 mathematics skills. Adolescents were recruited as they can handle the stress of fMRI
301 experimentation, are mathematically advanced enough and have had time to master the
302 subject area compared to younger children. This age range is also an advantageous time to
303 implement interventions to improve mathematical abilities before leaving school, hence adults
304 were not studied. EPT subjects were included to show that differences with patient populations
305 are detectable with our methods. A subsection of the full study is reported here to demonstrate
306 the real-time analysis.
307
308 The subjects made one two-hour visit to the MRI department at University Hospitals Cleveland
309 Medical Center (UHCMC). Ethics approval was obtained from the UHCMC Institutional Review
310 Board office prior to the study and complied with the Declaration of Helsinki for human subject
311 research. Subjects and their parents gave informed consent prior to taking part.
312
313 As part of our wider study, subjects also made another, separate 3 hour visit to the study
314 offices to undergo neuropsychological testing and a refresher of fraction calculations. In the
315 interests of brevity, the full neuropsychological testing results are not reported here. One
316 finding that is particularly relevant to the fMRI task considered here is that nearly two thirds
317 (63.6 %) of the EPT cohort have lower working memory function, compared to just over one
318 third (35.7 %) of controls subjects.
319
320 3.2 MRI protocols
321
322 The subjects were positioned head-first supine on the scanner bed with their head fixed in
323 position using inflatable pads. An 8-channel head coil was used for data acquisition. Echo planar
324 imaging scans were acquired on a Philips Ingenuity 3T PET/MR imager at UHCMC. The following
325 fMRI scan parameters were used: TR = 3.0 s, TE = 35 ms, in-plane resolution was 1.797 mm^2
326 (matrix 128 x 128), slice thickness was 4 mm, number of slices = 36 slices and flip angle = 90°. A
327 SENSE P reduction factor of 2 was implemented and scans were acquired in an ascending
328 interleaved fashion.
329
330 In addition to the fMRI scans, a high-resolution T1-weighted anatomical image of the brain was
331 also acquired. This was taken using a magnetic preparation gradient-echo sequence (3D IR TFE).
332 Imaging parameters were: TR = 7.5 ms, TE = 3.7 ms, in-plane resolution was 1 mm^2 (matrix 256
333 x 256), slice thickness was 1 mm, number of slices = 200 slices and flip angle = 8°.
334
335 3.3 Stimulus protocols
336
337 During data acquisition subjects were presented with a mathematical version of the well-known
338 1-back memory task. It involved performing basic addition and subtraction calculations and
339 required the answer to be remembered and compared to the next answer. Two difficulty levels
340 were included. The protocol was developed by our lab as part of a battery to assess
341 mathematical and working memory abilities in 14 – 17 year olds to evaluate the functional
342 differences between those born EPT and those born at normal term. The stimulus was

presented on an MRI compatible LCD monitor (manufactured by Cambridge Research Systems, Rochester, UK) positioned at the end of the bore and viewed via a mirror attached to the head coil. Equations were presented, for example, the subject may see "2 + 3 = ?". The subject was required to work out the answer and then remember it while working out the next equation, for example "1 + 4 = ?". If they thought the answers matched, then the subject pressed a button on a response box held in their right hand. If they thought the answers did not match, then they did nothing but remember the new answer to compare to the answer of the next equation. An example sequence is shown in Figure 1A.

The stimulus was presented in a block design, see Figure 1B and Table 1. Eight equations were presented per block. Each block lasted 36 seconds followed by 21 seconds of rest condition (fixation dot). Two difficulty levels were presented. The easier level consisted of single digit numbers to add or subtract and the answers were always a single digit. The harder level involved addition or subtraction of single or two-digit numbers and the answers were always two digits. Blocks of difficulty levels were alternated during the scan and a total of 6 blocks per level were presented. Note: although only 2 difficulty levels are used here, the setup is able to accommodate any number of difficulty levels. The full duration of the task was 238 scans or 11 minutes and 54 seconds. This was based on a moderate length of experimentation for a 1-back block design (e.g. see (32-35)), allowing approximately 6 minutes for each difficulty level.

Two difficulty levels were included to investigate differences in neural responses associated with increasing task demand. As the brain is 'pushed' to solve more complex problems, differential networks may be apparent, and these may be different between normal term and EPT subjects. Additionally, increasing the difficulty level serves to maintain the subject's attention and, generally, increases their effort. This can have the effect of increasing brain activation cluster sizes and magnitude as well as causing recruitment of additional areas, which is of interest. Incorporating difficulty levels into protocols that can be terminated early in a separate fashion demonstrates the flexibility of the proposed approach.

3.4 Real-time fMRI acquisition

The visual stimulus was presented using an in-house custom written program that was developed using the Python programming language (Python Software Foundation, https://www.python.org/) and libraries from Psychopy - an open source visual presentation program (36-38). The program connected to a Cedrus Lumina controller to receive stimulus responses from the subject and trigger pulses from the MRI scanner (outputted every dynamic). The timing of the presentation of the visual stimulus was synchronized to the trigger pulses to ensure that stimulus images were displayed at the expected time. A Supervisor Window displayed on the experimenter's computer screen allowed the visual stimulus to be tracked throughout. It displayed the current block number being presented, how many remaining blocks there were and when the subject responded. The program was also able to terminate one or both of the difficulty levels if it received a signal indicating the relevant areas in the fMRI data were sufficiently classified across voxels. The software is freely available from the Bitbucket repository: https://bitbucket.org/tatsuoka-lab/fmri-presentation.

Real-time image transfer was achieved by XTC (eXTernal Control). This is a program integrated into the Philips scanner software and enabled by a research clinical science key. XTC communicates with the reconstruction and scanner processes on the scanner computer and interfaces to a network Client application using a minimalistic CORBA (Common Object Request Broker Architecture) (39) interface which uses TCP/IP as the transport layer. CORBA is platform independent, reliable, and has the ability to process large amounts of data with minimum overhead. Each CORBA message consisted of a hierarchical attribute collection identified with UUIDs (universally unique identifiers) (40). Messages carried reconstructed image data and meta-data containing details of scan protocols. Due to hospital network security protocols the reconstructed images were placed in a folder on the scanner computer and then pushed across to a Linux computer. To achieve necessary image transfer speeds to the scanner computer folder a modification to XTC was installed on the scanner to disable two-way communications as only one-way image transfer functionality was required. However, XTC does support two-way communication between the scanner and the Client.

The Linux computer was a custom-built server equipped with a solid state hard drive and two 8-core Intel Xeon E5-2687W processors running at 3.1 GHz and providing 40 MB L3 cache. It was installed with Centos 7.4 operating system. As the scans were received, custom written Python and Bash scripts implemented the analysis using core-based parallelization to preprocess the data and perform the SPRT statistical analysis. Preprocessing was performed using standard modules from AFNI (Analysis of Functional NeuroImages, https://afni.nimh.nih.gov) and FSL (FMRIB's Software Library, https://fsl.fmrib.ox.ac.uk/fsl/fslwiki/). The analysis sequence is detailed in the following section. The setup is shown in Figure 2.

3.5 MRI preprocessing

At the beginning of the scanning session a single fMRI scan (3 seconds) was acquired and used for coregistration (motion correction) purposes. In preparation, the skull was removed using FSL's Brain Extraction Tool (BET) (41) and a mask of the full brain was created. During the real-time adaptive fMRI scan session, new scans arrived every 3 seconds and were dumped in a folder on the Linux workstation where the following actions were applied to each one. AFNI's 'dcm2niix_afni' command was used to convert the .par/.rec files to nifti. Motion correction was performed using coregistration techniques. Every fMRI scan was realigned to the initial scan that was acquired before the task began, and AFNI's '3dvolreg' command was used. Spatial smoothing was also applied using an 8 mm kernel with AFNI's '3dmerge' command. The full brain mask created at the beginning of the session was applied using FSL's 'fslmaths' command to remove noisy voxels outside the brain (voxels of no interest). The resulting images were then converted to ascii format for statistical analysis with SPRT.

3.6 fMRI SPRT analysis

The SPRT analysis was applied using highly-optimized C++ program that used Intel Cilk Plus library for multicore and vector processing of data. BLAS routines from Intel MKL were used to

enable instruction-based acceleration for matrix computation. They are available from the Bitbucket repository at https://bitbucket.org/tatsuoka-lab. The design matrix was created prior to the scan session using AFNI's '3dDeconvolve' command to model the stimulus and HRF. It is possible to include the temporal derivatives of the HRF or other regressors in the design matrix where applicable in studies. Temporal derivatives were not included here due to the long durations of the block design used to present the task. Statistical analysis included the modeling of low frequency physiological noise and the associated removal of serial correlation using discrete cosine transforms. Motion parameters are also frequently used as regressors to remove correlated activations produced by movement. Here motion parameter regressors were not included with the estimation of the discrete cosine transforms due to the limitations of the computational resources.

We also tested 2 scenarios using either 2-blocks or 4-blocks of easy and hard stimuli first stage administration before allowing early stopping to occur. Where 2-blocks per difficulty level of stimulus administration were used before allowing early stopping, the first 78 scans were used for the first stage of experimentation. Where 4-blocks were used, 154 scans were used for the first stage. Recall, a full-length task protocol comprised 238 scans and lasted 11 minutes and 54 seconds.

The automatic determination of when to terminate the scanning is based on the Type I and Type II errors, α_E and β_E, as described above. Typical values used in the literature were used to test stopping time performance, with $\alpha_E = 0.001$, $\beta_E = 0.1$ (42, 43). We also considered $\alpha_E = 0.0001$, $\beta_E = 0.1$ and $\alpha_E = 0.001$, $\beta_E = 0.01$ combinations as well. A percentage of voxels that must be classified before termination was also specified during the setup, such as 80%. We also evaluate 70% and 90% threshold levels.

This 1-back arithmetic task involves not only number sense and mathematical calculations but also general cognitive skills involving working memory and sustained attention. The brain networks involved with each of these has been well characterized in the literature and lends itself to the evaluation of this real-time analysis method. There is a large amount of overlap for the active brain areas that control each of these functions and they appear as a frontoparietal network (44-46). The areas of the brain we expect to see activate in response to the experimental task are: the intraparietal sulcus, supramarginal gyrus, premotor cortex, dorsal/ventral lateral prefrontal cortex, parietal lobe, Broca's area, occipital lobe, fusiform gyrus, precuneus, cingulate gyrus, anterior insula and frontal eye fields. Assessment of the location and extent of activations within this network will be used as additional criteria for judging appropriate stopping times, in addition to the statistical information determined through the SPRT analysis. This will include how well the cluster peaks coincide with the anatomical locations as well as their extent.

3.7 Group analysis

There are many possible applications in the research setting where individual level results may be the focus. A possible clinical application may be in clinical assessments for presurgical

evaluation for brain surgery in patients with brain cancer or epilepsy. Still, group analyses are commonly conducted and an essential aspect of fMRI analyses. The outputted results files from the SPRT analysis can be used directly to perform a group analysis using AFNI's 3dMEMA command (Mixed Effects Meta Analysis tool) (47). However, a group analysis was carried out using FSL which instead merges all subject data to conduct a combined mixed models analysis. We demonstrate that the data collected in real-time can still be used in a typical post-hoc analysis. Raw data was preprocessed with FSL FEAT (48). Motion correction was performed using a rigid body transform, spatial smoothing with a full-width-at-half-maximum Gaussian kernel of 6 mm was applied, high pass temporal filtering of 90 s was carried out and coregistration to (MNI) standard space was done before performing a first level individual GLM analysis. The statistical output from these were used to perform the higher level group statistics using FLAME 1 (FMRIB's Local Analysis of Mixed Effects, (49)).

4.0 Results

4.1 Individual Subject Results of SPRT

The median control subject response time across both difficulty levels was 1.44 sec (SD 0.51 sec), and median task accuracy was 90.8 % (SD 20.2 %). When these are broken down by difficulty level, the easy level median task accuracy was 86.1 % (SD 22.6 %) with median response time of 1.28 sec (SD 0.54 sec); and the hard level median task accuracy was 90.0 % (SD 18.4 %) with median response time of 1.56 sec (SD 0.51 sec). EPT subjects had a slightly longer overall median response time of 1.91 sec (SD 0.48 sec) and overall median task accuracy was lower at 65.8 % (SD 21.2 %). For the easy level, the median accuracy was 72.2 % (SD 24.2 %) and median response time was 1.63 sec (SD 0.49 sec). For the hard level the median accuracy was 70.0 % (SD 19.8 %) with a median response time of 2.10 sec (SD 0.54 sec). Note that there are statistically significant differences in same subject differences in speed to completion by difficulty level (Wilcoxon signed rank test, two-sided $p < 0.001$). Comparing correctness percentages per subject across birth status groups, there are significant differences with the hard level (Mann Whitney two-sided $p = 0.037$), but not with the easy one (two-sided $p = 0.401$). These results indicate that the difficulty levels have different psychometric properties, and affect the groups differently. We also see this in activation patterns, as discussed in Section 4.2 and reflected in the group analysis results.

Real-time transfer speeds between the scanner and the Linux computer were consistently fast, with individual scan files taking less than 150 milliseconds to transfer. All subject scans were processed within the 3 second TR period. Offline testing showed that the subject with the largest number of voxels (subject 21 with 135,379 voxels) was processed in just 5 minutes and 45 seconds, or 1.45 seconds per scan. The subject with the fewest number of voxels (subject 14 with 77,359 voxels) was processed in 5 minutes and 2 seconds, or 1.27 seconds per scan. Therefore, for the subject with the largest number of voxels, the maximum time to process 1 scan in real-time would be 1.6 sec (1.45 processing time + 0.150 transfer time). Thus, it is feasible for a TR of 2 seconds or faster to be used with the software, depending on transfer speeds and the number of voxels in the brain.

Inspection of the z-score maps for each subject showed that generally, across subjects, the largest activations were centered bilaterally around the inferior and superior parietal areas, taking in the intraparietal sulcus, a region highly associated with mathematical functioning. Further activations were seen in the cuneus. These are most likely correlated with the visual processing associated with the task. Additional activations were seen in the precuneus, bilateral areas in the medial frontal gyrus, anterior cingulate, insula and inferior frontal gyrus. These areas are often associated with attention and memory systems (44, 50).

The stopping times for the 2- and 4-block first stage lengths are reported in Table 2. First, as we see for instance in Figure 3, error variance estimate is not stable after a 2-block first stage. It is important to "wait" until this happens, as it plays a central role in inference and on test statistic values. The 4-block first stage is more attractive in this way. Table 3 shows how early stopping is affected by the SPRT Type I and Type II error threshold values. Note that early stopping does not occur for Type II error levels of 0.01 and is less affected by the Type I error specification.

Stopping was reached at 80% of voxels classified as either active or non-active in around 54% of cases in both scenarios for both difficulty levels. At 80% classification for control subjects, 7/12 subjects stopped early for the easy level with both the 2-block and 4-block first stages. For the hard level, 7/12 subjects with 2-blocks and 5/12 with 4-blocks stopped early. For EPT subjects, 6/11 subjects stopped early for the easy level for both 2- and 4-block first stage conditions. For the hard level, 5/11 subjects using 4-blocks as a minimum still stopped early and 7/12 subjects using 2-blocks as a minimum stopped early. The median stopping duration for both difficulty levels for control subjects was 3 blocks of easy and 2 blocks of hard stimulus administration for 2-blocks first stage. For 4-blocks first stage, the median stopping time was 5 easy, 4 hard for the easy level and 4 easy, 4 hard for the hard level. In EPT subjects, the median stopping time for 2-block first stage was 2 easy and 2 hard blocks of stimuli. For 4-blocks first stage, the median stopping time was 4 easy and 4 hard for both difficulty levels. Depending on the number of first stage blocks, time savings of 1/3 to 2/3 (4 to 8 minutes on a 12 minute scan) can be achieved.

An early stopping rule based on a classification rate of at least 70% or 90% was also tested. Results reported in Table 4. At 70% classification most subjects stopped early. For the 2-block first stage - easy level, only 3 out of 23 subjects did not stop early and for the hard level, 1 subject did not stop early. Median stopping scan number was 79 for both the easy and hard levels. For the 4-block first stage – easy level, 5/23 subjects did not stop early and 4/23 subjects did not stop early for the hard level. Median stopping scan was 155 for both difficulty levels. At 90% classification, there were very few instances when early stopping occurred. For the 2-blocks first stage condition, 3 subjects stopped early for the easy level and 1 subject for the hard level. Only 1 subject stopped early under the 4-blocks first stage condition for the easy level. A visual comparison of the activation maps for 70% and 80% voxel classification (see Table S1 in Supplemental Information) shows that in many instances there is little difference between the two stopping points. When analysing counts of voxels classified as active or non-active between these rules, the 80% thresholds lead to more non-active classifications, but the difference in active voxels is less systematic. Given that early stopping occurs almost invariably with the 70% rule, this criterion should also be considered. Table S2 provides plots of the

563 percentage of voxels that are respectively classified as active and non-active over the course of
564 the full scanning duration. A general trend is that the percentage of non-active voxels gradually
565 decreases while that of active voxels increases. Longer scan durations also may allow for some
566 adjustment of z-score activation thresholds in post-hoc analyses, and may have some potential
567 advantages for group analysis, as discussed below. Hence, we present results for the more
568 conservative 80% rule, which leads to relatively longer durations even when early stopping
569 occurs.
570
571 The activation maps under the different conditions are shown in Figure 4 for a sample subject
572 (subject 9). For the 2-block first stage, this subject terminated after 2 blocks of easy and hard
573 administration for the easy level (scan 79) and after 3 blocks of easy and 2 blocks of hard
574 administration for the hard level (scan 97). For the 4-block minimum, this subject terminated at
575 scan 155, equal to 4 blocks of easy and hard stimulus administration, for both difficulty levels.
576 The images show that at scan 79 there is very little activity present and the majority of the
577 voxel classifications are non-active. By scan 155, there is much more activity which has a similar
578 pattern to the final scan. The extent is not quite as large as the final scan, however the foci of
579 the clusters do overlap between the two time points. As mentioned, this is likely due to the
580 alternative hypothesis threshold $c'\beta$ value corresponding to relatively lower z-score values as
581 the number of scans increase. This pattern of 'growing' activations for given alternative
582 hypothesis $c'\beta$ over scan duration is thus typical of our early stopping data, particularly for the
583 2-block initial stage. Visual inspection of the z-score maps at the stopping scan for other
584 subjects revealed similar patterns. In most instances, the additional active voxels at full
585 duration were around the edges of existing clusters at the early stopping scans. Further images
586 of other subjects are presented in Table S1 in the Supplementary Information document. Plots
587 of the percentage of active and non-active voxels classified at each scan are given in Table S2 of
588 the same document. The overlaps between early stopping and full duration maps are also
589 explored further in Table 2 where we show the number of active voxels in common spatially
590 between the two durations. Although some of these show less than 50% overlap with the final
591 scan, it can be seen that this is due to the smaller cluster sizes with early stopping. The median
592 spatial overlap where early stopping occurs for control subjects was 27.9% (SD 30.2%) for the
593 easy level, 2-blocks and 68.5% (SD 15.4%) for the easy level, 4-blocks. For the hard level, there
594 was 26.0% (SD 19.9%) and 44.6% (SD 21.3%) for the 2-block and 4-block first stages,
595 respectively. For EPT subjects the median overlap was 34.2% (SD 34.0%) and 33.5% (SD 34.3%)
596 for the easy level, 2- and 4-block first stages, respectively. For the hard level, the median
597 overlap values were 14.6% (SD 9.4%) and 77.6% (SD 25.2%) for 2-block and 4-block first stages.
598
599 This phenomenon is basically driven by the estimation variance of the GLM parameters steadily
600 decreasing as more scans are accrued, while at the same time the alternative hypothesis z-
601 score threshold is being held the same. Given that estimated beta and error variance values
602 essentially become stable in most cases, voxel-level z-scores will increase. This leads to
603 increasingly larger number of voxels being classified as active. We assessed a sample of the
604 error variance estimates over scan duration, as in Figure 3. We illustrate similarities in
605 activation patterns with early stopping and full duration if the z-score threshold increases as the
606 scan durations increase. Assuming no serial correlation as an approximation, note that the

variance of $\hat{\beta}$ is $(\sigma)^2(X'X)^{-1}$ where X is the known design matrix. $(X'X)^{-1}$ is thus known as well for all scans, and it decreases as scan duration increases. Stopping early at a given threshold can thus be similar to stopping later with a stricter threshold for activation, provided error variance and beta parameter estimates stabilize, which we assess for with the first stage. A z-score of 3.1 for 154 scans approximately corresponds to a z-score of 4.0 for the final scan (228 scans). At 78 scans, a z-score of 3.1 corresponds to a z-score of approximately 8.37 and 5.92 for the easy and hard task parameter respectively, so there will be even less overlap, even if the z-score threshold is 4.0 at full duration. See Table S1 in the Supplement for images resulting from different stop rules and first stage durations. In Table S2, the trends in percentage of voxels classified as active and non-active reflect this phenomenon, at least for some of the subjects.

Importantly, the issue of whether early stopping or full duration provide better activation maps is best answered neuroscientifically, through the support of literature and hypotheses. In the Supplement, we add plots for early stopping versus full duration for each subject for which early stopping was invoked. Comparing these plots, we see that in many instances that the cluster peaks are located in the expected anatomical locations. However, at full duration results, numerous voxels with lower z-scores appear around the edges of the clusters and extend well beyond the anatomical boundaries of the gyri indicating areas of activation in white matter and cerebrospinal fluid. This suggests that these lower z-score voxels are more likely to be false positives as scan duration increases, as argued above, and indicates that scanning for full duration doesn't necessarily improve the results.

In summary, although there are similar rates of early termination between the 2-block and 4-block first stage cases, the detected activation patterns suggest that using 4-blocks of stimulus administration is more suited to determining active voxels. In Figure 3, to illustrate the rate of decrease of the estimated σ_t^2 values, we present a plot of $\widehat{\sigma_t}$ values for one subject across a set of voxels over the duration of the experiment. These values give an indication that stopping based on the θ-values at the end of the 2-block first stage may be too early for correspondence with full duration scans, as the estimated standard deviations are relatively larger. This implies that the alternative hypotheses can have much larger θ-values early on compared to full duration, while this difference in θ-values is less after 4-blocks. Note that in some subjects there is some volatility due to subject movement. Below, we consider full duration z-score thresholds of 4.0 versus early stopping results with a threshold of 3.1, so that activation magnitudes considered as active are more comparable. See also, Table 5 comparing the overlap in cluster locations and extent from full duration z = 4.0 with early stop scan z = 3.1.

In all but three EPT subjects the active voxel count increases with scan duration. Subjects 13, 15 and 17 are the exception. Subject 13 demonstrates very few active voxels at all and there is almost no consistency in location. Further investigation shows large relative framewise displacement occurs frequently throughout the scan and many of the responses have been missed or have relatively long response times, 60.5% correct overall and 2.08 s (SD 0.97 s) average response time (see plots for subject 13 in Table S3 of Supplementary Information document). Taken together these suggest that either the task level may not have been aimed at

the right level and/or the subject may have been uncomfortable and distracted in the scanner thereby attending to the task less than required for robust activations to occur. Subject 15 demonstrates cluster sizes that decrease over time. Framewise displacement shows very little motion, particularly from scan 180 onwards. The response plots (in Table S3 of Supplementary Information) show the subject is paying attention and responding appropriately. Subject 17 has a similar pattern of decreasing cluster sizes. The framewise displacement plots indicate a moderate amount of motion throughout. Although the subject has missed many of the task questions (65.8% correct), the pattern of responding indicates they are awake and attending to the task. In general, EPT subjects demonstrated more motion. The median number of scans with framewise displacement above a threshold of 0.9 mm, threshold determined from (51), was 5 scans (SD 43 scans) for EPT subjects and 2.5 scans (SD 8 scans) for control subjects. One EPT subject passed the threshold a total of 124 scans out of 238 scans. In contrast, the control subject with the maximum number of threshold passes was 30/238 scans. This is further demonstrated in Figure 5 where we show subject counts for each scan when the threshold has been passed. For both EPT and control subjects, it is clear that subjects are moving more frequently in the second half of the scans and supports stopping early to reduce motion artifacts and noise in the data. Formally, we see statistically significant differences when comparing counts of motion events with framewise displacement greater than 0.9mm in the first versus second half of scanning ($p= 0.003$, two-sided signed rank test). EPT group also has significantly more movement in the first half of scanning ($p= 0.035$, two-sided Mann-Whitney test), indicating a group-level proclivity for more motion events.

4.2 Group Analysis Results

The results for the 1-back easy and hard contrasts for the 2- and 4-block first stage conditions for EPT and control subjects are shown in Figure 6. Location of activity is listed in Table S4 of the Supplementary Information. The group results of full scan durations are compared to the group results using only the scans up to the early stopping point for each subject for each difficulty level and number of blocks completed before early stopping was allowed. We examined within group differences as well as between group differences. The EPT > control and control > EPT contrasts did not show any differences with the full duration and early stopped scans, which could in part be due to sample size limitations and the within group heterogeneity of the EPT group. The focus for the results here are within group for the easy and hard levels.

The control subjects show strong activations in the anterior cingulate and bilateral parietal regions, see Tables 6 and S4, and Figure 6. The easy and hard 4-block first stage scans appear similar to the final scans. There is less correspondence between the 2-block first stage scans and the final scans, reflecting the individual results reported above. The EPT group easy level scans are consistent across all stages but there is more variability in the activations across the hard level. Across all EPT scans, there is more right sided activity compared to controls. This is discussed below.

5.0 Discussion

Based on analysis of a training sample, we have presented a workflow for the implementation of an adaptive real-time fMRI system that allows for statistically-driven dynamic adjustment of experimentation based on voxel-level SPRT. We show that this dynamic and adaptive statistical approach is generally comparable to corresponding fixed experimental designs in terms of detected activation, particularly when adjusting for stricter z-score thresholds for full scan to account for reduced estimation variance. At the same time, time savings in experiment durations can be substantial. Moreover, with respect to individual data, as scans increased, we observed that more and more of the newly classified active voxels were located around the edges of clusters in many subjects. For some, clusters would even merge into one larger cluster across the brain that would consist of 10,000's of voxels. This effect was addressed by the work of Saad et al. (2003) who investigated the effect of the number of time points on the extent of brain activations. They observed a similar effect that longer scanning potentially increases the detection of false positives but not the detection of true positives (52).

We explored imposing two different first stage lengths before early stopping is considered using either 2- or 4-blocks each of easy and hard stimulus administration. The 4-block first stage is justified over the 2-block because of the comparative stability of the estimation of error variances and other GLM parameters. In contrast, for the 2-block first stage, parameter estimation can be more variable. Also, correspondence in early-stop activation patterns to full scan duration requires very high z-score threshold adjustments, which may be too stringent to detect important activations. The 2-block first stage often led to most voxels being classified as non-active. See Table S2. While the 4-block first stage provides less opportunity for efficiency gains, as the window for early stopping is narrower, but it is more prudent given the need for parameter estimates to stabilize. It is possible that a 3-block initial stage could provide comparable results as the 4-block initial stage, but this was not explored here.

In the SPRT framework, other α_E, β_E- pairs were considered as well, to test how different combinations impact activity detection and early stopping. For instance, given selection of α_E = 0.001 and β_E = 0.01, overall stopping did not occur. In this case, the more stringent choice of β_E makes it more difficult to cross either of the SPRT thresholds. We also saw that for either α_E = 0.001 or α_E = 0.0001 being paired with β_E = 0.1, early stopping occurred for both of the experimental conditions, with somewhat faster early stopping for the less stringent α_E.

In terms of the global stop rule threshold, we observed that for the cases under consideration, stopping when 80% of voxels in the full brain (or smaller ROI) respectively satisfy their SPRT-based stopping criterion generally leads to early stopping of stimulus administration, while also leading to comparable activation classification as with the full protocol, after z-test score threshold adjustment for scan duration. The stricter 90% criterion was infrequently satisfied, and did not often lead to early stopping of experimentation. Recall that when GLM parameter values are "in-between" the null and alternative hypothesis values, SPRT-based stopping is less likely at the voxel level. A 100% stopping rule is thus not feasible, as are values relatively close to 100%. This phenomenon becomes less of an issue with more scans, since θ_t, the alternative

hypothesis threshold for $c'\beta$, decreases in value as more scans are accrued, given the z-score threshold of 3.10 is held constant. Fewer voxels are then "in-between". The 80% rule seems conservative in that not all participants are stopped early, but there are high levels of correspondence in individual and group level activation maps with full durations, particularly when the first stage is comprised of 4 blocks, and the full scan z-score is adjusted. The 70% rule is more aggressive, and early stopping is invoked at a much higher rate. Given that the resultant images from early stopping in many cases appear similar across these two rules, the 70% rule should be considered as well.

The SPRT approach was effective at detecting brain activity at the individual level with early stopping in both the control and EPT groups. Note the individual variability among subjects in early stopping performance. Factors that can affect stopping times include the magnitudes of activation, variability in task performance, sustained attention levels, motion, and the noise levels in the BOLD signal. Those born EPT also can have structural abnormalities of the brain which can affect fMRI results and 2 subjects reported here had clear abnormalities that were obvious even in this low resolution data. Less obvious abnormalities may have been present in some of the other subjects.

The EPT group data demonstrated more right sided activity and smaller cluster sizes by comparison to control group data across all stopping points. In order to understand this result it is necessary to consider neuropsychological skills and structural and functional brain changes within the group. Working memory is a key skill required for both mathematics and this numerical 1-back task. Recall the lower accuracy and longer response times in the EPT group. fMRI studies on dyscalculia (difficulty in learning and performing mathematics) suggest that there is greater heterogeneity in activations with a more diffuse pattern being apparent (53, 54). Additionally, there is overlap in structural differences in white matter integrity, as measured from diffusion weighted imaging studies, between those born EPT and those with dyscalculia including inferior fronto-occipital fasciculus and the inferior and superior longitudinal fasciculi (55-58). These connect crucial areas associated with mathematics and working memory. A more diffuse and variable pattern of functional activity, perhaps partly due to structural differences, may confound a group analysis in this instance. More data points from individuals do seem to improve the results, perhaps allowing the variability to dampen somewhat. This is supported by the change in variance for the group between early stopping with 2- and 4-block first stages and full duration analyses, see right-hand column of Table 6. The control group variances are relatively much lower throughout, as the extremely pre-mature birth group was neurologically and cognitively more heterogeneous. If group-level analysis is a main objective, it is possible that groups could be treated differently in how early stopping is approached based on within-group heterogeneity and the need for more scan data to help overcome this. This issue needs further investigation.

With this data, a group analysis was feasible using the early stopping data in controls. A possible limitation was discovered in performing a group analysis of the EPT group, as these subjects demonstrated greater variability in location at the individual level. While it is feasible to apply our approach for patient group studies, consideration should be given to the particular

patient groups of interest and the likely within group differences in brain activity when making the decision to stop early. We conjecture that larger sample sizes or stricter early stopping criteria may help overcome larger variability.

In the future, it is possible that the first stage length can be tailored at the voxel level, once it is clear error variance and other GLM parameter estimates are relatively stable, which is expected at some point due to the convergence properties of the estimators. This may facilitate earlier stopping. Alternatively, if local computational resources are limited, note that stopping can be assessed on an interval basis, and not necessarily after every scan. Although not considered here, these BOLD signal-based early stopping rules could also possibly be enriched by incorporating individual motion displacement patterns, as well as behavioural measures such as correctness rates in experimentation.

Here we demonstrated full brain analytics with parallelization using MKL Intel libraries for matrix computation with two Xeon E5-2687W 8-core processors. It is also feasible to consider only partial brain volumes where experiments demand more consideration of a particular area. Future directions for the study are to implement the SPRT and Bayesian sequential estimation methods using distributed computing approaches to increase processing speed allowing full brain real-time analyses and advance stopping rule methods in shorter scan times.

6.0 Conclusion

We introduce a systematic, statistically-based approach to dynamic experimentation with real-time fMRI. Saving in scan time and accurate voxel activation detection can be achieved, while redundant experimentation in block design is reduced. We investigate different aspects of how to determine early stopping rules. These analyses can be viewed as intended on a training sample to guide implementation of early stopping in future studies involving the same experiments and study populations. These methods lay a foundation for future dynamic experimentation approaches and early stopping rules with real-time fMRI, including for resting state and neural feedback. Use of high performance computing will enable the advent of more sophisticated real-time experimental designs and dynamically determined early stopping rules.

Declaration of conflicts of interest: All authors declare no conflicts of interest.

Author contributions

SC – Study design, analysis and interpretation of data, drafting of manuscript
WC – Study design, analysis and interpretation of data, software development, drafting of manuscript
JF – Study design and software development
HF – Study design and technical support, drafting of manuscript
JSG – Software development, review of manuscript
JZ – Analysis and interpretation of data, review of manuscript
CT – Study design, analysis and interpretation of data, drafting of manuscript

Funding: This study was supported by Phillips Healthcare and the National Science Foundation (Award number: 1561716).

Acknowledgements
None

Data availability

The raw data supporting the conclusions of this article will be made available by the authors, without undue reservation.

References

1. A. A. Alegria, M. Wulff, H. Brinson, G. J. Barker, L. J. Norman, D. Brandeis, D. Stahl, A. S. David, E. Taylor, V. Giampietro and K. Rubia: Real-Time fMRI Neurofeedback in Adolescents with Attention Deficit Hyperactivity Disorder. *Human Brain Mapping*, 38(6), 3190-3209 (2017) doi:10.1002/hbm.23584
2. M. S. Sherwood, J. H. Kane, M. P. Weisend and J. G. Parker: Enhanced control of dorsolateral prefrontal cortex neurophysiology with real-time functional magnetic resonance imaging (rt-fMRI) neurofeedback training and working memory practice. *Neuroimage*, 124, 214-223 (2016) doi:10.1016/j.neuroimage.2015.08.074
3. E. J. Lawrence, L. Su, G. J. Barker, N. Medford, J. Dalton, S. C. R. Williams, N. Birbaumer, R. Veit, S. Ranganatha, J. Bodurka, M. Brammer, V. Giampietro and A. S. David: Self-regulation of the anterior insula: Reinforcement learning using real-time fMRI neurofeedback. *Neuroimage*, 88, 113-124 (2014) doi:10.1016/j.neuroimage.2013.10.069
4. C. Hohenfeld, N. Nellessen, I. Dogan, H. Kuhn, C. Muller, F. Papa, S. Ketteler, R. Goebel, A. Heinecke, N. J. Shah, J. B. Schulz, M. Reske and K. Reetz: Cognitive Improvement and Brain Changes after Real-Time Functional MRI Neurofeedback Training in Healthy Elderly and Prodromal Alzheimer's Disease. *Frontiers in Neurology*, 8 (2017) doi:10.3389/fneur.2017.00384
5. L. Subramanian, J. V. Hindle, S. Johnston, M. V. Roberts, M. Husain, R. Goebel and D. Linden: Real-Time Functional Magnetic Resonance Imaging Neurofeedback for Treatment of Parkinson's Disease. *Journal of Neuroscience*, 31(45), 16309-16317 (2011) doi:10.1523/jneurosci.3498-11.2011
6. L. Subramanian, M. B. Morris, M. Brosnan, D. L. Turner, H. R. Morris and D. E. J. Linden: Functional Magnetic Resonance Imaging Neurofeedback-guided Motor Imagery Training and Motor Training for Parkinson's Disease: Randomized Trial. *Frontiers in Behavioral Neuroscience*, 10 (2016) doi:10.3389/fnbeh.2016.00111
7. S. Lui, X. H. J. Zhou, J. A. Sweeney and Q. Y. Gong: Psychoradiology: The Frontier of Neuroimaging in Psychiatry. *Radiology*, 281(2), 357-372 (2016) doi:10.1148/radiol.2016152149
8. K. Vakamudi, C. Trapp, K. Talaat, K. X. Gao, B. S. D. Guimaraes and S. Posse: Real-Time Resting-State Functional Magnetic Resonance Imaging Using Averaged Sliding Windows with Partial Correlations and Regression of Confounding Signals. *Brain Connectivity*, 10(8), 448-463 (2020) doi:10.1089/brain.2020.0758

9. R. W. Cox, A. Jesmanowicz and J. S. Hyde: REAL-TIME FUNCTIONAL MAGNETIC-RESONANCE-IMAGING. *Magnetic Resonance in Medicine*, 33(2), 230-236 (1995) doi:10.1002/mrm.1910330213

10. R. Goebel: BrainVoyager - Past, present, future. *Neuroimage*, 62(2), 748-756 (2012) doi:10.1016/j.neuroimage.2012.01.083

11. J. R. Sato, R. Basilio, F. F. Paiva, G. J. Garrido, I. E. Bramati, P. Bado, F. Tovar-Moll, R. Zahn and J. Moll: Real-Time fMRI Pattern Decoding and Neurofeedback Using FRIEND: An FSL-Integrated BCI Toolbox. *Plos One*, 8(12) (2013) doi:10.1371/journal.pone.0081658

12. J. J. Yoo, O. Hinds, N. Ofen, T. W. Thompson, S. Whitfield-Gabrieli, C. Triantafyllou and J. D. E. Gabrieli: When the brain is prepared to learn: Enhancing human learning using real-time fMRI. *Neuroimage*, 59(1), 846-852 (2012) doi:10.1016/j.neuroimage.2011.07.063

13. O. Hinds, S. Ghosh, T. W. Thompson, J. J. Yoo, S. Whitfield-Gabrieli, C. Triantafyllou and J. D. E. Gabrieli: Computing moment-to-moment BOLD activation for real-time neurofeedback. *Neuroimage*, 54(1), 361-368 (2011) doi:10.1016/j.neuroimage.2010.07.060

14. M. T. Debettencourt, J. D. Cohen, R. F. Lee, K. A. Norman and N. B. Turk-Browne: Closed-loop training of attention with real-time brain imaging. *Nature Neuroscience*, 18(3), 470-165 (2015) doi:10.1038/nn.3940

15. R. Lorenz, R. P. Monti, I. R. Violante, C. Anagnostopoulos, A. A. Faisal, G. Montana and R. Leech: The Automatic Neuroscientist: A framework for optimizing experimental design with closed-loop real-time fMRI. *Neuroimage*, 129, 320-334 (2016) doi:10.1016/j.neuroimage.2016.01.032

16. R. Lorenz, I. R. Violante, R. P. Monti, G. Montana, A. Hampshire and R. Leech: Dissociating frontoparietal brain networks with neuroadaptive Bayesian optimization. *Nature Communications*, 9 (2018) doi:10.1038/s41467-018-03657-3

17. I. J. Feng, A. I. Jack and C. Tatsuoka: Dynamic Adjustment of Stimuli in Real Time Functional Magnetic Resonance Imaging. *Plos One*, 10(3) (2015) doi:10.1371/journal.pone.0117942

18. M. Jenkinson, C. F. Beckmann, T. E. Behrens, M. W. Woolrich and S. M. Smith: FSL. *Neuroimage*, 62(2), 782-790 (2012) doi:10.1016/j.neuroimage.2011.09.015

19. N. Lazar: The Statistical Analysis of Functional MRI Data. Springer-Verlag New York, (2008) doi:10.1007/978-0-387-78191-4

20. R. W. Cox: AFNI: Software for analysis and visualization of functional magnetic resonance neuroimages. *Computers and Biomedical Research*, 29(3), 162-173 (1996) doi:10.1006/cbmr.1996.0014

21. R. J. Carroll, S. Wang, D. G. Simpson, A. J. Stromberg and D. Ruppert: The Sandwich (Robust Covariance Matrix) Estimator. In: Texas A&M University, (1998)

22. G. Kauermann and R. J. Carroll: A note on the efficiency of sandwich covariance matrix estimation. *Journal of the American Statistical Association*, 96(456), 1387-1396 (2001) doi:10.1198/016214501753382309

23. K. J. Friston, O. Josephs, E. Zarahn, A. P. Holmes, S. Rouquette and J. B. Poline: To smooth or not to smooth? Bias and efficiency in fMRI time-series analysis. *Neuroimage*, 12(2), 196-208 (2000) doi:10.1006/nimg.2000.0609

24. C. Yan, D. Liu, Y. He, Q. Zou, C. Zhu, X. Zuo, X. Long and Y. Zang: Spontaneous brain activity in the default mode network is sensitive to different resting-state conditions with limited cognitive load. *PLoS One*, 4(5), e5743 (2009) doi:10.1371/journal.pone.0005743

25. A. Wald: Sequential Analysis. John Wiley and Sons, (1947)

26. A. Wald and J. Wolfowitz: OPTIMUM CHARACTER OF THE SEQUENTIAL PROBABILITY RATIO TEST. *Annals of Mathematical Statistics*, 19(3), 326-339 (1948) doi:10.1214/aoms/1177730197

27. D. R. Cox: Large Sample Sequential Tests for Composite Hypotheses. *The Indian Journal of Statistics, Series A (1961-2002)*, 25(1), 5-12 (1963)

28. S. Tantaratana and J. B. Thomas: TRUNCATED SEQUENTIAL PROBABILITY RATIO TEST. *Information Sciences*, 13(3), 283-300 (1977) doi:10.1016/0020-0255(77)90050-0

29. J. X. Li: Sequential probability ratio tests for generalized linear mixed models. In: University of California, Riverside, (2010)

30. J. B. T. Sawasd Tantaratana: Truncated sequential probability ratio test. *Information Sciences*, 13(3), 283-300 (1977) doi:http://dx.doi.org/10.1016/0020-0255(77)90050-0

31. W. J. Hall: SOME SEQUENTIAL ANALOGS OF STEINS 2-STAGE TEST. *Biometrika*, 49(3-4), 367-& (1962) doi:10.1093/biomet/49.3-4.367

32. X. Di, H. M. Zhang and B. B. Biswal: Anterior cingulate cortex differently modulates frontoparietal functional connectivity between resting-state and working memory tasks. *Human Brain Mapping*, 41(7), 1797-1805 (2020) doi:10.1002/hbm.24912

33. J. Z. Huang, L. Xie, R. W. Guo, J. H. Wang, J. Q. Lin, Z. B. Sun, S. X. Duan, Z. R. Lin, H. Li and S. H. Ma: Abnormal brain activity patterns during spatial working memory task in patients with end-stage renal disease on maintenance hemodialysis: a fMRI study. *Brain Imaging and Behavior* (2020) doi:10.1007/s11682-020-00383-7

34. M. Daamen, J. G. Bauml, L. Scheef, C. Sorg, B. Busch, N. Baumann, P. Bartmann, D. Wolke, A. Wohlschlager and H. Boecker: Working Memory in Preterm-Born Adults: Load-Dependent Compensatory Activity of the Posterior Default Mode Network. *Human Brain Mapping*, 36(3), 1121-1137 (2015) doi:10.1002/hbm.22691

35. G. R. Poudel, J. C. Stout, J. F. Dominguez, M. A. Gray, L. Salmon, A. Churchyard, P. Chua, B. Borowsky, G. F. Egan and N. Georgiou-Karistianis: Functional changes during working memory in Huntington's disease: 30-month longitudinal data from the IMAGE-HD study. *Brain Structure & Function*, 220(1), 501-512 (2015) doi:10.1007/s00429-013-0670-z

36. J. W. Peirce: PsychoPy - Psychophysics software in Python. *Journal of Neuroscience Methods*, 162(1-2), 8-13 (2007) doi:10.1016/j.jneumeth.2006.11.017

37. J. W. Peirce: Generating stimuli for neuroscience using PsychoPy. *Frontiers in Neuroinformatics*, 2 (2009) doi:10.3389/neuro.11.010.2008

38. J. Peirce and M. MacAskill: Building Experiments in Pscychopy. Sage Publications Ltd, London, England (2018)

39. D. C. Schmidt, D. L. Levine and S. Mungee: The design of the TAO real-time object request broker. *Computer Communications*, 21(4), 294-324 (1998) doi:10.1016/s0140-3664(97)00165-5

40. ITU-T: Series X: Data Networks and Open System Communications. In: Ed I. T. S. S. o. ITU. ISO/IEC, (2005)

41. S. M. Smith: Fast robust automated brain extraction. *Human Brain Mapping*, 17(3), 143-155 (2002) doi:10.1002/hbm.10062

42. H. R. Cremers, T. D. Wager and T. Yarkoni: The relation between statistical power and inference in fMRI. *Plos One*, 12(11) (2017) doi:10.1371/journal.pone.0184923

43. A. Banerjee, U. B. Chitnis, S. L. Jadhav, J. S. Bhawalkar and S. Chaudhury Hypothesis testing, type I and type II errors. *Industrial Psychiatry Journal*, 18, 127-131 (2009) doi:0.4103/0972-6748.62274

44. V. Menon: Memory and cognitive control circuits in mathematical cognition and learning. *Mathematical Brain across the Lifespan*, 227, 159-186 (2016) doi:10.1016/bs.pbr.2016.04.026

45. V. Menon: Working memory in children's math learning and its disruption in dyscalculia. *Current Opinion in Behavioral Sciences*, 10, 125-132 (2016) doi:10.1016/j.cobeha.2016.05.014

46. W. J. Chai, A. I. Abd Hamid and J. M. Abdullah: Working Memory From the Psychological and Neurosciences Perspectives: A Review. *Frontiers in Psychology*, 9 (2018) doi:10.3389/fpsyg.2018.00401

47. G. Chen, Z. S. Saad, A. R. Nath, M. S. Beauchamp and R. W. Cox: FMRI group analysis combining effect estimates and their variances. *Neuroimage*, 60(1), 747-765 (2012) doi:10.1016/j.neuroimage.2011.12.060

48. M. W. Woolrich, B. D. Ripley, M. Brady and S. M. Smith: Temporal autocorrelation in univariate linear modeling of FMRI data. *Neuroimage*, 14(6), 1370-1386 (2001) doi:10.1006/nimg.2001.0931

49. M. W. Woolrich, T. E. J. Behrens, C. F. Beckmann, M. Jenkinson and S. M. Smith: Multilevel linear modelling for FMRI group analysis using Bayesian inference. *Neuroimage*, 21(4), 1732-1747 (2004) doi:10.1016/j.neuroimage.2003.12.023

50. A. E. Cavanna and M. R. Trimble: The precuneus: a review of its functional anatomy and behavioural correlates. *Brain*, 129, 564-583 (2006) doi:10.1093/brain/awl004

51. J. S. Siegel, J. D. Power, J. W. Dubis, A. C. Vogel, J. A. Church, B. L. Schlaggar and S. E. Petersen: Statistical improvements in functional magnetic resonance imaging analyses produced by censoring high-motion data points. *Human Brain Mapping*, 35(5), 1981-1996 (2014) doi:10.1002/hbm.22307

52. Z. S. Saad, K. M. Ropella, E. A. DeYoe and P. A. Bandettini: The spatial extent of the BOLD response. *Neuroimage*, 19(1), 132-144 (2003) doi:10.1016/s1053-8119(03)00016-8

53. K. Kucian, T. Loenneker, T. Dietrich, M. Dosch, E. Martin and M. von Aster: Impaired neural networks for approximate calculation in dyscalculic children: a functional MRI study. *Behav Brain Funct* . 2, 31 (2006) doi:10.1186/1744-9081-2-31

54. M. M. Berl, C. J. Vaidya and W. D. Gaillard: Functional imaging of developmental and adaptive changes in neurocognition. *Neuroimage*, 30(3), 679-691 (2006) doi:10.1016/j.neuroimage.2005.10.007

55. I. M. Loe, J. N. Adams and H. M. Feldman: Executive Function in Relation to White Matter in Preterm and Full Term Children. *Frontiers in Pediatrics*, 6 (2019) doi:10.3389/fped.2018.00418

56. J. M. Young, B. R. Morgan, H. E. A. Whyte, W. Lee, M. L. Smith, C. Raybaud, M. M. Shroff, J. G. Sled and M. J. Taylor: Longitudinal Study of White Matter Development and Outcomes in

Children Born Very Preterm. *Cerebral Cortex*, 27(8), 4094-4105 (2017) doi:10.1093/cercor/bhw221

57. E. Rykhlevskaia, L. Q. Uddin, L. Kondos and V. Menon: Neuroanatomical correlates of developmental dyscalculia: combined evidence from morphometry and tractography. *Frontiers in Human Neuroscience*, 3 (2009) doi:10.3389/neuro.09.051.2009

58. K. Kucian, S. S. Ashkenazi, J. Hanggi, S. Rotzer, L. Jancke, E. Martin and M. von Aster: Developmental dyscalculia: a dysconnection syndrome? *Brain Structure & Function*, 219(5), 1721-1733 (2014) doi:10.1007/s00429-013-0597-4

Figure 1: A) Sample 1-back protocols demonstrating the two difficulty levels. B) Block design and timings of each difficulty level.

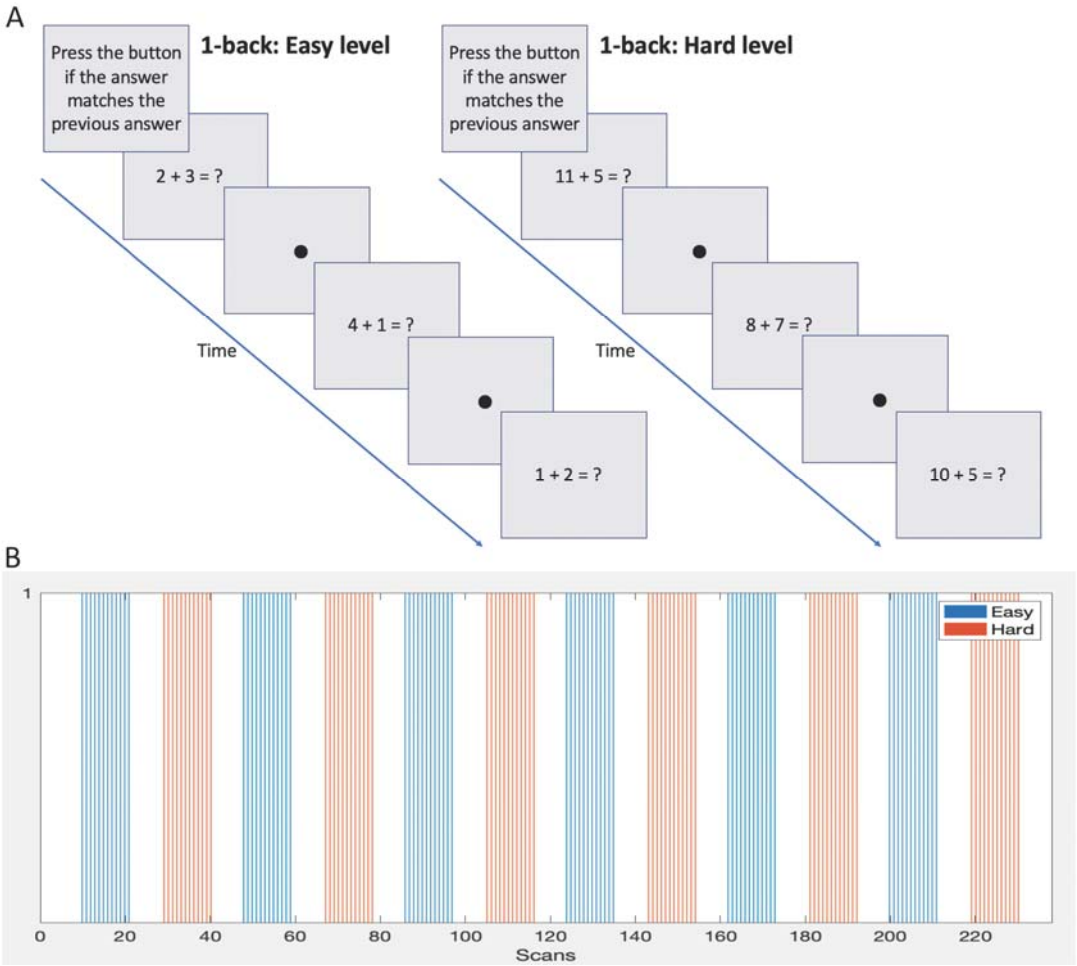

Figure 2: Schematic of the experimental setup of the dynamic real-time fMRI process. The equations were presented to the subject while the scans were acquired using a dedicated computer. FMRI scans were exported in real-time from the scanner computer to the Linux workstation using the Philips XTC program and CORBA interface. Scans were preprocessed on the Linux workstation and SPRT statistics were calculated. The results were relayed back to the stimulus presentation program with an instruction to either continue or terminate the stimulus.

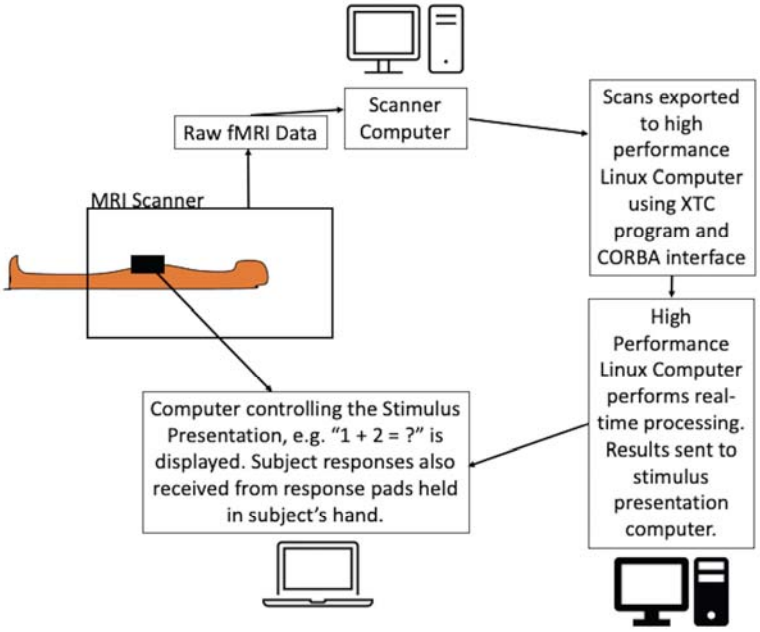

Figure 3: Estimated standard deviations for $c_1\widehat{\beta}$. Plots for 3 sample active (bottom) and non-active (top) voxels from a control subject (subject 3) showing how the estimates decrease over time (scan number).

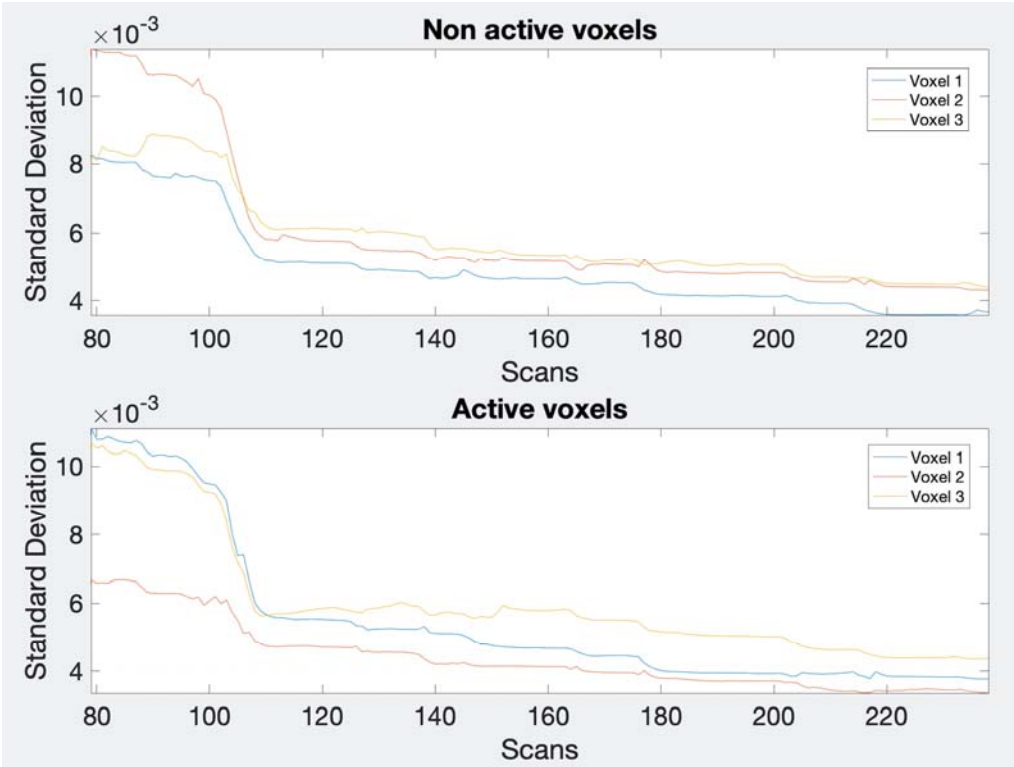

Figure 4: Full brain activation maps showing the overlapping voxels between the different stopping points (using 2-blocks first stage, 4-blocks first stage and final scan). Top row shows the easy level and bottom row shows the hard level for 1 subject (number 9). The active voxels that are active only at full duration are shown in blue. Those only active after 2-blocks or 4-blocks of stimulus administration are in red. Yellow shows the overlap between full duration and 2-block first stage early stopping scans. Green shows the overlap between full duration and 4-block first stage stopping scans. $P \leq 0.001$ uncorrected, $z > 3.1$. Right hand images show the comparison of 4-blocks early stopping with $z > 3.1$ with full duration that has been thresholded at $z > 4.0$. Light blue indicates overlapping voxels. Results overlaid on MNI template, slice z = 56 shown. R = right, A = anterior.

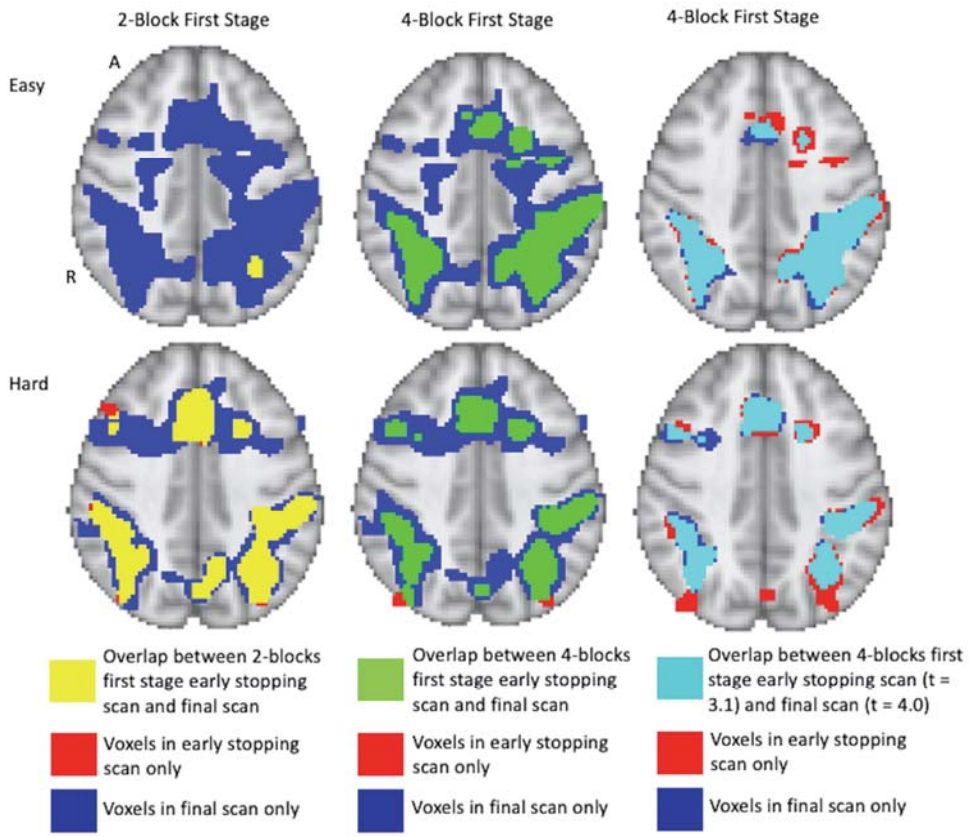

Figure 5: Plots showing the number of subjects that pass the framewise displacement threshold of 0.9 mm for each scan. Top: EPT subjects, bottom: control subjects.

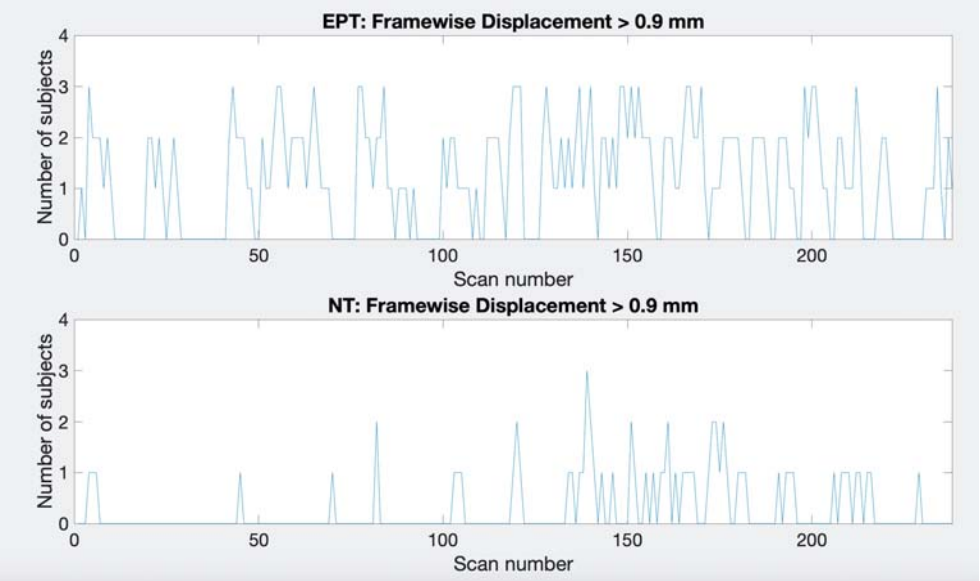

Figure 6: Group results for the 1-back task. Analysis performed for controls and EPT subjects using FSL. Early stopping with 2- and 4-blocks being initially administered is compared to full duration. Activations are overlaid on the MNI template brain. Red (A) = easy level results, Blue (B) hard level results. P < 0.001 uncorrected. Slices z = 58 is shown. R = right, L = left, A = anterior, P = posterior.

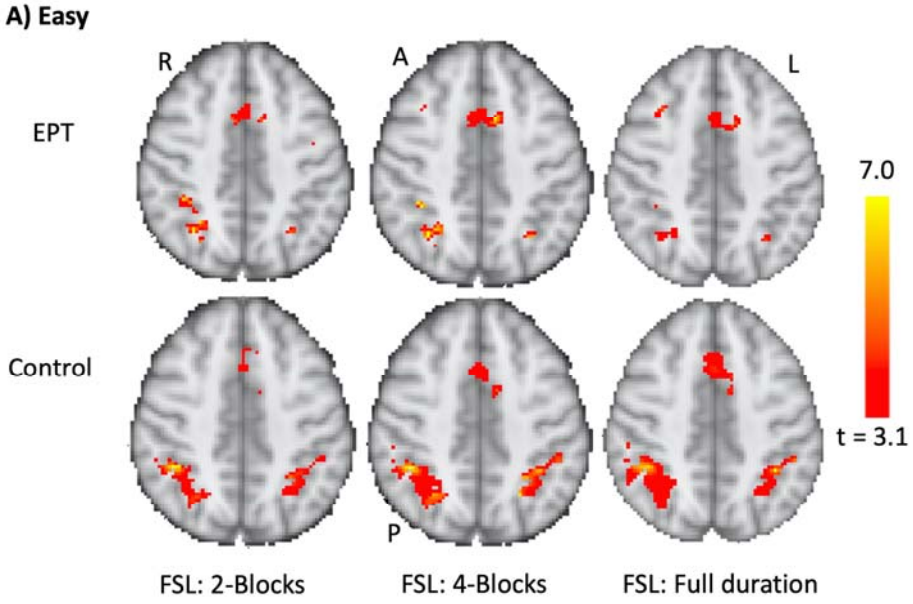

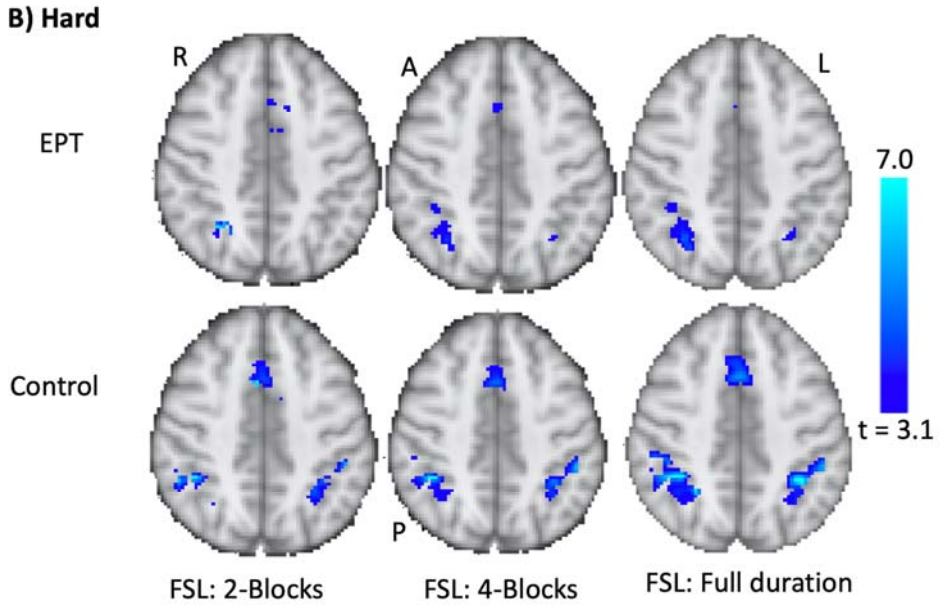

Table 1: The scan number when each stimulus block is completed.

Block	Easy level	Hard level
1	21	40
2	59	78
3	97	116
4	135	154
5	173	192
6	211	230

Table 2: Subject results of the 1-back task using SPRT to analyse the data. Analysis reported here uses $\alpha_E = 0.001$, $\beta_E = 0.1$ and thresholded at $p < 0.001$. A) Easy level: 2-block, B) Hard level: 2-block, C) Easy level: 4-block and D) Hard level: 4-block. After each subject's last administered block, the number of active voxels that spatially overlap between early stopping and full duration are given. The percentage of voxels-in-common is also given relative to the total number of active voxels at the full duration scan. Maximum number of possible scans is 238, minimum is 78 scans for 2 blocks first stage of easy and hard stimulus administration or 154 scans for 4 blocks first stage of easy and hard. Median values are calculated with those who stopped early only. Information given for the point where 80% of voxels have been classified as either active or non-active. N/A = not applicable.

A) Easy level – 2 block first stage

Subject	**Scan when 80% Reached**	**% overlap**	**No of Voxels Classified Active at 80%**	**No of Voxels Classified Active at Final Scan**	**Voxels in Scan at Early Stopping but not Final Scan**	**Voxels in Final Scan but not Scan at Early Stopping**	**No of Voxels in ROI (full brain)**

Control							
1	Not reached	100	3,556	3,556	N/A	N/A	115,062
2	Not reached	100	12,803	12,803	N/A	N/A	113,564
3	3E/3H	39.2	5,379	13,472	96	8,189	77,359
4	Not reached	100	13,680	13,680	N/A	N/A	103,591
5	5E/5H	69.4	7,482	10,540	170	3,228	114,260
6	2E/2H	9.2	979	4,674	547	4,242	121,353
7	3E/3H	27.9	1,394	4,115	246	2,967	107,406
8	5E/5H	81.3	7,068	7,124	1,278	1,334	106,267
9	2E/2H	1.0	349	9,329	257	9,237	121,195
10	Not reached	100	7,340	7,340	N/A	N/A	96,565
11	3E/2H	19.4	1,597	6,357	363	5,123	107,016
12	Not reached	100	12,429	12,429	N/A	N/A	96,936
EPT							
13	2E/2H	0.0	59	49	59	49	94,623
14	6E/6H	95.2	15,556	15,866	445	755	94,905
15	4E/4H	36.1	1,014	750	743	479	98,799
16	Not reached	100	13,484	13,484	N/A	N/A	118,098
17	2E/2H	34.2	4,723	3,487	3,531	2,295	124,749
18	2E/2H	8.8	717	3,925	373	3,581	97,437
19	Not reached	100	7,402	7,402	N/A	N/A	135,379
20	2E/2H	16.3	1,361	8,093	39	6,771	89,609
21	Not reached	100	10,039	10,039	N/A	N/A	104,584
22	Not reached	100	13,817	13,817	N/A	N/A	114,201
23	Not reached	100	6,715	6,715	N/A	N/A	86,177

B) Hard level – 2 blocks first stage

Subject	**Scan when 80% Reached**	**% overlap**	**No of Voxels Classified Active at 80%**	**No of Voxels Classified Active at Final Scan**	**Voxels in Scan at Early Stopping but not Final Scan**	**Voxels in Final Scan but not Scan at Early Stopping Scan**	**No of Voxels in ROI (full brain)**
Control							
1	Not reached	100	23,351	23,351	N/A	N/A	115,062
2	Not reached	100	20,749	20,749	N/A	N/A	113,564
3	2E/2H	23.1	3,478	14,976	18	11,516	77,359
4	3E/2H	43.1	5,986	9,874	1,735	5,623	103,591
5	2E/2H	24.2	3,743	14,939	135	11,331	114,260
6	4E/3H	71.6	6,129	7,829	527	2,227	121,353
7	3E/2H	9.6	330	2,494	91	2,255	107,406
8	Not reached	100	14,634	14,634	N/A	N/A	106,267
9	3E/2H	31.9	3,253	8,898	412	6,057	121,195

10	3E/2H	26.0	4,948	10,921	2,114	8,087	96,565
11	Not reached	100	11,355	11,355	N/A	N/A	107,016
12	Not reached	100	29,279	29,279	N/A	N/A	96,936
EPT							
13	79	0.0	133	860	133	860	94,623
14	2E/2H	33.8	7,676	21,074	546	13,944	94,905
15	3E/2H	12.3	892	1,696	684	1,488	98,799
16	Not reached	100	14,984	14,984	N/A	N/A	118,098
17	2E/2H	20.3	1,796	4,335	918	3,457	124,749
18	Not reached	100	10,967	10,967	N/A	N/A	97,437
19	2E/2H	6.7	1,274	7,609	761	7,096	135,379
20	2E/2H	16.9	1,535	8,754	53	7,272	89,609
21	2E/2H	12.3	2,415	10,038	1,181	8,638	104,584
22	Not reached	100	15,374	15,374	N/A	N/A	114,201
23	Not reached	100	8,088	8,088	N/A	N/A	86,177

C) Easy level – 4 blocks first stage

Subject	**No of Easy/Hard blocks when 80% Reached**	**% overlap**	**No of Voxels Classified Active at 80%**	**No of Voxels Classified Active at Final Scan**	**Voxels in Scan at Early Stopping but not Final Scan**	**Voxels in Final Scan but not Scan at Early Stopping**	**No of Voxels in ROI (full brain)**
Control							
1	Not reached	100	3,556	3,556	N/A	N/A	115,062
2	Not reached	100	12,803	12,803	N/A	N/A	113,564
3	5E/4H	77.6	10,921	13,472	471	3,022	77,359
4	Not reached	100	13,680	13,680	N/A	N/A	103,591
5	5E/5H	69.4	7482	10,540	170	3228	114,260
6	5E/5H	68.5	3,806	4,674	603	1,471	121,353
7	5E/4H	50.9	2,195	4,115	99	2,019	107,406
8	5E/5H	81.3	7,068	7,124	1,278	1,334	106,267
9	4E/4H	42.2	4,065	9,329	127	5,391	121,195
10	Not reached	100	7,340	7,340	N/A	N/A	96,565
11	5E/5H	47.9	3,088	6,357	40	3,309	107,016
12	Not reached	100	12,429	12,429	N/A	N/A	96,936
EPT							
13	4E/4H	95.2	139	49	136	46	94,623
14	6E/6H	33.5	15,556	15,866	445	755	94,905
15	4E/4H	100	899	750	648	499	98,799
16	Not reached	77.7	13,484	13,484	N/A	N/A	118,098
17	6E/6H	31.1	3,908	3,487	1,199	778	124,749
18	4E/4H	100	1,302	3,925	80	2,703	97,437
19	Not reached	14.3	7,402	7,402	N/A	N/A	135,379

20	4E/4H	100	1,302	8,093	148	2,898	89,609
21	Not reached	100	10,039	10,039	N/A	N/A	104,584
22	Not reached	100	13,817	13,817	N/A	N/A	114,201
23	Not reached	100	6,715	6,715	N/A	N/A	86,177

D) Hard level – 4 blocks first stage

Subject	**Scan when 80% Reached**	**% overlap**	**No of Voxels Classified Active at 80%**	**No of Voxels Classified Active at Final Scan**	**Voxels in Scan at Early Stopping but not Final Scan**	**Voxels in Final Scan but not Scan at Early Stopping**	**No of Voxels in ROI (full brain)**
Control							
1	Not reached	100	23,351	23,351	N/A	N/A	115,062
2	Not reached	100	20,749	20,749	N/A	N/A	113,564
3	6E/5H	87.4	13,160	14,976	67	1,883	77,359
4	Not reached	100	9,874	9,874	N/A	N/A	103,591
5	Not reached	100	14,939	14,939	N/A	N/A	114,260
6	5E/4H	71.6	6,129	7,829	527	2,227	121,353
7	4E/4H	40.6	1,214	2,494	202	1,482	107,406
8	Not reached	100	14,634	14,634	N/A	N/A	106,267
9	4E/4H	44.6	4,313	8,898	343	4,928	121,195
10	4E/4H	40.8	5,360	10,921	908	6,469	96,565
11	Not reached	100	11,355	11,355	N/A	N/A	107,016
12	Not reached	100	29,279	29,279	N/A	N/A	96,936
EPT							
13	4E/4H	45.0	1,919	860	1,532	473	94,623
14	4E/4H	84.8	20,638	21,074	2,774	3,210	94,905
15	Not reached	100	1,696	1,696	N/A	N/A	98,799
16	Not reached	100	14,984	14,984	N/A	N/A	118,098
17	6E/6H	78.0	4,482	4,335	1,101	954	124,749
18	Not reached	100	10,967	10,967	N/A	N/A	97,437
19	4E/4H	26.9	3,397	7,609	1,353	5,565	135,379
20	4E/4H	77.6	8,107	8,754	1,312	1,959	89,609
21	Not reached	100	10,038	10,038	N/A	N/A	104,584
22	Not reached	100	15,374	15,374	N/A	N/A	114,201
23	Not reached	100	8,088	8,088	N/A	N/A	86,177

Table 3: Comparison of stopping times using $\alpha_E = 0.001$ and $\alpha_E = 0.0001$. Based on 80% of voxels being classified. Both 2-block and 4-block first stage conditions are presented. A) Easy and hard level: 2-block, B) Easy and hard level: 4-block.

A) 2-block first stage

Easy	**Hard**

Subject	α_E = 0.001, β_E = 0.1,	α_E = 0.0001, β_E = 0.1,	α_E = 0.001, β_E = 0.1,	α_E = 0.0001, β_E = 0.1,
Control				
1	Not reached	Not reached	Not reached	Not reached
2	Not reached	Not reached	Not reached	Not reached
3	104	215	79	79
4	Not reached	Not reached	89	99
5	178	Not reached	79	79
6	79	79	166	196
7	112	138	95	95
8	177	181	Not reached	Not reached
9	79	79	86	86
10	Not reached	Not reached	98	101
11	89	89	Not reached	Not reached
12	Not reached	Not reached	Not reached	Not reached
EPT				
13	79	79	79	79
14	230	Not reached	79	Not reached
15	154	154	87	87
16	Not reached	Not reached	Not reached	Not reached
17	79	79	79	79
18	79	79	Not reached	Not reached
19	Not reached	Not reached	79	79
20	79	79	79	79
21	Not reached	Not reached	79	80
22	Not reached	Not reached	Not reached	Not reached
23	Not reached	Not reached	Not reached	Not reached

B) 4-block first stage

	Easy		**Hard**	
Subject	α_E = 0.001 β_E = 0.01	α_E = 0.0001, β_E = 0.1,	α_E = 0.001 β_E = 0.01	α_E = 0.0001, β_E = 0.1,
Control				
1	Not reached	Not reached	Not reached	Not reached
2	Not reached	Not reached	Not reached	Not reached
3	171	215	200	Not reached
4	Not reached	Not reached	Not reached	Not reached
5	178	Not reached	Not reached	Not reached
6	180	202	166	196
7	164	164	155	155
8	177	181	Not reached	Not reached
9	155	155	155	155

10	Not reached	Not reached	155	Not reached
11	186	197	Not reached	Not reached
12	Not reached	Not reached	Not reached	Not reached
EPT				
13	155	155	155	155
14	230	Not reached	155	Not reached
15	155	155	Not reached	Not reached
16	Not reached	Not reached	Not reached	Not reached
17	216	216	218	224
18	155	155	Not reached	Not reached
19	Not reached	Not reached	155	155
20	155	155	155	160
21	Not reached	Not reached	Not reached	Not reached
22	Not reached	Not reached	Not reached	Not reached
23	Not reached	Not reached	Not reached	Not reached

Table 4: A comparison of the early stopping times at 70%, 80% and 90% of voxels classified as either active or non-active. Conducted using $\alpha_E = 0.001$, $\beta_E = 0.1$. Both 2-block and 4-block first stage conditions are presented. A) Easy and hard level: 2-block, B) Easy and hard level: 4-block.

A) 2-block first stage

	Easy			**Hard**		
Subject	**Scan when 70% reached**	**Scan when 80% reached**	**Scan when 90% reached**	**Scan when 70% reached**	**Scan when 80% Reached**	**Scan when 90% reached**
Control						
1	147	Not reached	Not reached	79	Not reached	Not reached
2	79	Not reached	Not reached	80	Not reached	Not reached
3	89	104	Not reached	79	79	Not reached
4	144	Not reached	Not reached	79	89	Not reached
5	79	132	Not reached	79	79	Not reached
6	79	79	79	86	166	Not reached
7	79	112	Not reached	80	95	Not reached
8	140	177	Not reached	98	Not reached	Not reached
9	79	79	79	79	86	Not reached
10	79	Not reached	Not reached	79	98	Not reached
11	79	89	Not reached	Not reached	Not reached	Not reached
12	79	Not reached	Not reached	79	Not reached	Not reached
EPT						
13	79	79	111	79	79	79
14	84	230	Not reached	79	79	Not reached
15	107	154	Not reached	79	87	Not reached
16	Not reached	Not reached	Not reached	109	Not reached	Not reached
17	79	79	Not reached	79	79	Not reached

18	79	79	Not reached	197	Not reached	Not reached
19	79	Not reached	Not reached	79	79	Not reached
20	79	79	Not reached	79	79	Not reached
21	Not reached	Not reached	Not reached	79	79	Not reached
22	Not reached	Not reached	Not reached	79	Not reached	Not reached
23	203	Not reached	Not reached	79	Not reached	Not reached

B) 4-block first stage

	Easy			**Hard**		
Subject	**Scan when 70% reached**	**Scan when 80% reached**	**Scan when 90% reached**	**Scan when 70% reached**	**Scan when 80% Reached**	**Scan when 90% reached**
Control						
1	155	Not reached	Not reached	161	Not reached	Not reached
2	Not reached	Not reached	Not reached	155	Not reached	Not reached
3	155	171	Not reached	155	200	Not reached
4	155	Not reached	Not reached	155	Not reached	Not reached
5	155	177	Not reached	155	Not reached	Not reached
6	155	180	Not reached	158	166	Not reached
7	155	164	Not reached	155	155	Not reached
8	155	177	Not reached	155	Not reached	Not reached
9	155	155	Not reached	155	Not reached	Not reached
10	155	Not reached	Not reached	155	155	Not reached
11	155	186	Not reached	Not reached	Not reached	Not reached
12	Not reached	Not reached	Not reached	Not reached	Not reached	Not reached
EPT						
13	155	155	178	155	158	Not reached
14	155	230	Not reached	155	Not reached	Not reached
15	155	155	Not reached	155	Not reached	Not reached
16	Not reached	Not reached	Not reached	155	Not reached	Not reached
17	155	216	Not reached	155	218	Not reached
18	155	155	Not reached	197	Not reached	Not reached
19	155	Not reached	Not reached	155	155	Not reached
20	155	155	Not reached	155	159	Not reached
21	Not reached	Not reached	Not reached	Not reached	Not reached	Not reached
22	Not reached	Not reached	Not reached	Not reached	Not reached	Not reached
23	203	Not reached	Not reached	155	Not reached	Not reached

Table 5: Overlap with full duration scan threshold of z = 4.0. The 2- and 4-block first stage results are thresholded at z = 3.1. The percentage of voxels-in-common is also given relative to the total number of active voxels at the full duration scan. Median values are calculated with those who stopped early only. N/A = not applicable.

A) Easy level

Subject	2-Blocks % overlap	Voxels in Scan at Early Stopping but not Final Scan	Voxels in Final Scan but not Scan at Early Stopping	4-Blocks % overlap	Voxels in Final Scan but not Scan at Early Stopping	Voxels in Scan at Early Stopping but not Final Scan	No of Voxels Classified Active at Final Scan
Control							
1	100	N/A	N/A	100	N/A	N/A	1,099
2	100	N/A	N/A	100	N/A	N/A	8,166
3	47.6	229	5,668	88.0	1,297	1,400	10,818
4	100	N/A	N/A	100	N/A	N/A	8,535
5	93.7	1,178	426	93.7	426	1,178	6,730
6	14.2	610	2,229	87.7	319	1,527	2,598
7	42.1	420	1,339	75.4	569	451	2,313
8	95.1	3,232	199	95.1	199	3,232	4,035
9	0.9	297	5,784	62.8	2,172	401	5,836
10	100	N/A	N/A	100	N/A	N/A	4,077
11	25.1	721	2,611	78.7	742	343	3,487
12	100	N/A	N/A	100	N/A	N/A	7,413
EPT							
13	0	59	0	0	0	139	0
14	74.9	3,502	0	74.9	0	3,502	16,095
15	80.6	927	21	81.5	20	811	108
16	100	N/A	N/A	100	N/A	N/A	7,887
17	44.6	4,119	749	97.9	28	2,583	1,353
18	12.2	480	1,706	56.8	839	198	1,943
19	100	N/A	N/A	100	N/A	N/A	3,582
20	20.7	79	4,920	13.6	1,315	456	6,202
21	100	N/A	N/A	100	N/A	N/A	2,816
22	100	N/A	N/A	100	N/A	N/A	8,102
23	100	N/A	N/A	100	N/A	N/A	4,654

B) Hard level

Subject	2-Blocks % overlap	Voxels in Scan at Early Stopping but not Final Scan	Voxels in Final Scan but not Scan at Early Stopping	4-Blocks % overlap	Voxels in Final Scan but not Scan at Early Stopping	Voxels in Scan at Early Stopping but not Final Scan	No of Voxels Classified Active at Final Scan
Control							

1	100	N/A	N/A	100	N/A	N/A	15,071
2	100	N/A	N/A	100	N/A	N/A	13,253
3	28.0	68	8,787	98.9	138	1,101	12,197
4	51.4	2,613	3,193	100	N/A	N/A	6,566
5	33.1	314	6,938	100	N/A	N/A	10,367
6	88.1	1,609	611	88.1	611	1,609	5,131
7	15.4	146	1,009	71.0	346	367	1,193
8	100	N/A	N/A	100	N/A	N/A	9,802
9	44.5	590	3,321	60.8	2,344	673	5,984
10	34.5	2,828	4,027	59.8	2,473	1,686	6,147
11	100	N/A	N/A	100	N/A	N/A	6,331
12	100	N/A	N/A	100	N/A	N/A	20,299
EPT							
13	0	133	191	65.4	66	1,794	191
14	40.7	1,120	9,539	93.8	995	5,538	16,095
15	27.1	748	388	100	N/A	N/A	532
16	100	N/A	N/A	100	N/A	N/A	11,257
17	30.9	1,207	1,317	98.9	21	2,597	1,906
18	100	N/A	N/A	100	N/A	N/A	5,975
19	9.6	980	2,777	45.2	1,682	2,008	3,071
20	21.5	79	5,331	87.6	844	2,164	6,787
21	18.3	1,503	4,075	100	N/A	N/A	4,987
22	100	N/A	N/A	100	N/A	N/A	9,937
23	100	N/A	N/A	100	N/A	N/A	5,744

Table 6: The number of active voxels that spatially overlap between early stopping and full duration group analyses are listed. Images thresholded at $p < 0.001$. The percentage of voxels-in-common is given relative to the total number of active voxels detected at full duration. Stopping based on 80% classification at the individual level.

	No of Active Voxels	**Voxels in Scan at Early Stopping but not Final Scan**	**Voxels in Final Scan but not in Scan at Early Stopping**	**% of Common Voxels with Final Scan**	**Standard Deviation Values**
EPT - Easy					
2-Blocks	743	478	263	50.2	2,183
4-Blocks	839	466	155	70.6	1,385
Full duration	528				1,135
EPT - Hard					
2-Blocks	633	377	930	21.6	2,209
4-Blocks	1,002	225	155	65.5	1,170
Full duration	1,186				1,054

Controls - Easy					
2-Blocks	2,065	730	941	58.7	640
4-Blocks	2,882	1,150	409	76.1	857
Full duration	2,276				469
Controls – Hard					
2-Blocks	2,691	1,535	1,364	45.9	1,008
4-Blocks	2,433	789	876	65.2	743
Full duration	2,520				685